รายงานวิจัยฉบับสมบูรณ์

โครงการจมูกอิเล็กทรอนิกส์แบบไฮบริดที่พัฒนาจากก๊าซเซ็นเซอร์แบบโลหะออกไซด์ร่วมกับก๊าซเซ็นเซอร์แบบนาโนคอมโพสิตเพื่อใช้ในการระบุชนิดของแบคทีเรีย

โดย ผู้ช่วยศาสตราจารย์ดร. สุมนา กลัดสมบูรณ์

พฤศจิกายน พ.ศ. 2563

(ทุนพัฒนาศักยภาพในการทำงานวิจัยของอาจารย์รุ่นใหม่)

สัญญาเลขที่

MRG6080151

รายงานวิจัยฉบับสมบูรณ์

โครงการจมูกอิเล็กทรอนิกส์แบบไฮบริดที่พัฒนาจากก๊าซเซ็นเซอร์แบบโลหะออกไซด์ร่วมกับก๊าซเซ็นเซอร์แบบนาโนคอมโพสิตเพื่อใช้ในการระบุชนิดของแบคทีเรีย

ผู้ช่วยศาสตราจารย์ดร. สุมนา กลัดสมบูรณ์
คณะเทคนิคการแพทย์ มหาวิทยาลัยมหิดล

สนับสนุนโดยสำนักงานกองทุนสนับสนุนการวิจัยและต้นสังกัด

รูปแบบ Abstract (บทคัดย่อ)

Project Code: MRG6080151

(รหัสโครงการ)

Project Title: Hybrid electronic nose based on metal- oxide semiconductor and nanocomposite gas sensors for bacterial identification

(ชื่อโครงการ) จมูกอิเล็กทรอนิกส์แบบไฮบริดที่พัฒนาจากก๊าซเซ็นเซอร์แบบโลหะออกไซด์ร่วมกับก๊าซเซ็นเซอร์แบบนาโนคอมโพสิตเพื่อใช้ในการระบุชนิดของแบคทีเรีย

Investigator: Asst. Prof. Dr. Sumana Kladsomboon,
Faculty of Medical Technology, Mahidol University

E-mail Address: sumana.kla@mahidol.edu

Project Period: 3 years

(ระยะเวลาโครงการ)

1. Abstract

Bacterial infection commonly occurs in patient who has other disease. Conventional technique for bacterial identification, i.e., cell culture, takes time at least 24-48 hours and needs specialist to identify. Therefore, the screening method based on electronic nose (E-nose) was interested. This technique classifies vapor sample using two main components, namely, gas sensor and pattern recognition. Firstly, two types of gas sensor e.g. optical gas sensor (in optical e-nose system) and nanocomposite gas sensor (in electrical e-nose system) were developed based on organic-inorganic dyes such as metallo-porphyrin and metallo-phthalocyanine. Next, the optical and electrical e-nose systems were proposed to predict the pathogenic bacterial species based on the volatile organic compound (VOC) from bacteria in culture medium. Thus, a comparative evaluation of volatile fingerprint from five bacterial species such as *E. cloacae, E. coli, P. aeruginosa, S. aureus* and *S. Typhi.* grown in Luria-Bertani medium was conducted to determine the effect of incubation time on the yield of volatile biomarkers to discriminate bacterial from other. Finally, based on a pattern recognition technique, we found that the proposed optical gas sensor and electrical gas sensor can discriminate the pathogenic bacteria odor and the consequent VOCs-odor pattern of each bacterium depend on the different phases of bacterial growth.

Keywords: electronic nose; metallo-porphyrin; metallo-phthalocyanine; pattern recognition; bacterial discrimination

2. Objective

2.1 To study the interaction energies and electronic properties between organic-inorganic dyes and VOCs molecule using density functional theory calculation (DFT)

2.2 To develop the hybrid gas sensor platform for nanocomposite gas sensor and metal oxide semiconductor gas sensors in e-nose setup

2.3 To develop the gas sensor based on organic-inorganic dyes and carbon nanotube for VOCs detection

2.4 To apply the e-nose system for the bacterial identification

3. Experimental

3.1 To study the interaction energies and electronic properties between organic- inorganic dyes and VOCs molecule using density functional theory calculation (DFT)

The ability of binding between porphyrin and phthalocyanine with VOC was investigated by using molecular calculation based on density functional theory (DFT). This calculation is the versatile methods to calculate the electronic structure for instance bond distance, bond angles, interaction energy and atomic charge. The optimized distance between sensing molecules and analyte molecules were investigated by DFT calculation at the basic set B3LYP/6-31G* level based on single point optimization. The interaction energy (E_{Int}) between sensing molecules (porphyrin and phthalocyanine) and VOC molecule were calculated by varying the distance between metal atom of sensing molecules and oxygen atom of VOC molecules. The interaction energy (E_{Int}) was obtained by equation (1) :

$$E_{Int} = E_{SM+VOC} - (E_{SM} + E_{VOC}) \quad (1)$$

where E_{SM} and E_{VOC} are the total energy of the isolated sensing molecule and isolated VOC molecule, respectively. E_{SM+VOC} is the total energy when sensing molecule interact with VOC molecule. In this study, the targeted molecules from bacterial activity were aldehyde, acid, ketone, alcohol, amine and sulfide.

3.2 Develop the hybrid gas sensor platform for nanocomposite gas sensor and metal oxide semiconductor gas sensors in e-nose setup

This hybrid electronic nose system involves four main elements: sensor chamber, controller circuit, odor delivery sections and data acquisition (DAQ) as shown in Figure 1. The list of gas sensor arrays is presented in Table 1. In this work, there were 2 types of gas sensor, i.e. metal-oxide semiconductor (MOS) and nanocomposite gas sensors. Six gas sensors were placed in sensor chamber which is made from Teflon material. There

was gas inlet hole at the center of the bottom plates (top view of Figure 1). The controller circuit provided current for both MOS and nanocomposite gas sensors. Moreover, the controller circuit managed the solenoid valves to punctuate between VOC (or sample) and pure air (or reference gas) for gas delivering into sensor chamber. For the odor delivery sections, the sample bottle was the commercial glasses (100 ml Schott, Duran) with polypropylene screw caps and pouring rings. The temperature of sample bottle was controlled by heated bath during the experiment. Pure air or air zero was used as the carrier gas to deliver the sample gas into the sensor chamber. The flow rate of pure air was controlled by commercial flor meter. National Instruments data acquisition (Ni-DAQ) USB-6008 card with LabVIEW was chosen for measurement and control all device (analog input and digital output), see Figure 1. Moreover, the sensor signal, i.e. resistance change of gas sensor, was delivered to the computer by DAQ.

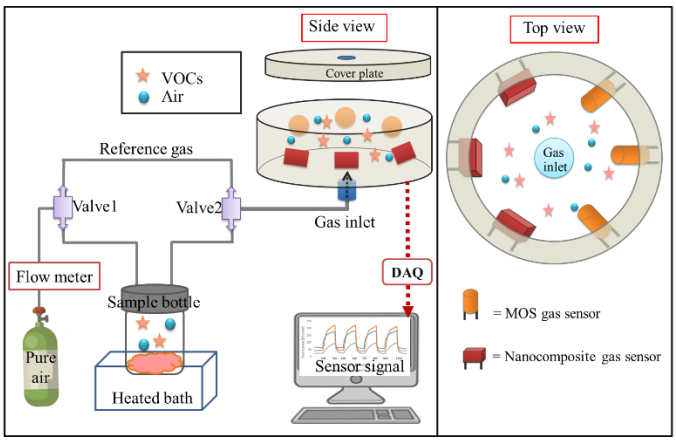

Figure 1 The hybrid electronic nose system using the organic-inorganic nanocomposites gas sensors coupled with MOS gas sensors.

Table1: The gas sensor arrays and their electrical resistivity.

Sensor no.	Gas sensor	Resistance (kΩ)
1	ZnTPP-MCNT	4
2	ZnF16Pc-MCNT	0.5
3	CuTTBPc-MCNT	42
4	ZnTPP-MCNT	9
5	CoTPP-MCNT	5
6	TGS 2444	140
7	TGS 2603	250
8	TGS2620	120

3.3 To develop the gas sensor based on organic-inorganic dyes and carbon nanotube for VOCs detection

The developed gas sensors were tested by the major VOCs in bacterial growing phase such as acetic acid, acetone, ammonia, ethanol, ethyl acetate and formaldehyde. Moreover, the gas sensors' sensitivity under the dynamic gas flow condition was investigated by artificial nose system. In this work, two types of gas sensor, namely, optical gas sensor and nanocomposite gas sensor were parallel developed. The detail of both sensors are presented as follow:

3.3.1 Optical gas sensor

Optical gas sensor fabrication

The organic-inorganic optical gas sensor was fabricated from Zinc-5,10,15,20-tetra-phenyl-21H,23H-porphyrin (ZnTPP), zinc-2,9,16,23-tetra-tert-butyl-29H, 31H-phthalocyanine (ZnTTBPc), and manganese (III)-5,10,15,20-tetraphenyl-21H,23H-porphyrin chloride (MnTPPCl). The ZnTPP, ZnTTBPc, and MnTPPCl were dissolved in chloroform at the concentrations 5, 10 and 15 mg/mL, respectively. Then, equal volumes of the three solutions were mixed together. Next, 0.5 mL of the mixed solution was deposited on clean glass substrates, using the spin coating method at a speed of 1,000 rpm for 30 s. Finally, the sensing films were treated by thermal treatment for 30 min at 150 °C under air atmosphere.

Characterization of the optical gas sensor

Change of optical absorption spectra of gas sensors for both the non-treated and treated sensing films were investigated with a UV-Vis spectrophotometer. The optical gas sensors were placed into a stable VOC atmosphere chamber to observe their sensitivity by six vapors: acetic acid, acetone, ammonia, ethanol, ethyl acetate, and formaldehyde. The absorption index of gas sensors when tested along with each VOC were recorded in the visible spectral range of 300-700 nm. Moreover, the optical gas sensors' sensitivity under dynamic gas flow conditions was investigated by an optical artificial nose system. All tested VOC solutions were prepared at the concentration of 10% (volume/volume) in water. Once a VOC sample was incorporated into a sample bottle, the operating temperature was adjusted for each VOC sample to control for the same evaporating pressure of each VOC through the sensor chamber. In addition, a nitrogen carrier system was installed inside the system to spread the VOC's vapor evenly across the bottle, delivering volatile vapors to the sensor chamber. Two cases of the non-treated and treated gas sensors were consecutively exposed to the VOCs for 2 min and N_2 for 2 min at room

temperature. Lastly, structure and morphology of the gas sensor were measured by atomic force microscopy

Optical artificial nose system

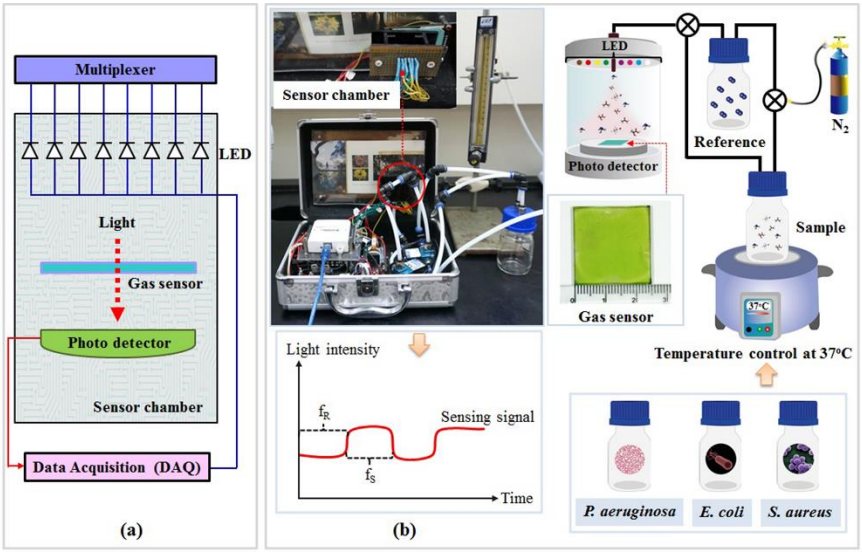

Figure 2. Schematic diagram of the optical artificial nose system, including (a) measurement/controller circuit section and (b) odor delivery section.

In this work, the optical artificial nose system was used to investigate the sensors' sensitivity under dynamic gas flow conditions. The schematic diagram of the in-house artificial nose system is shown in Figure 2. This system involves two main elements: measurement/controller circuit section and odor delivery section. A National Instruments data acquisition (Ni-DAQ) USB-6008 card with LabVIEW was chosen as the measurement and the control device, see Figure 2a. Low cost commercial LED lamps were used to create an artificial light source. Each channel of the analog multiplexer selected one of several input signals from individual LED lamps and forwarded the selected input into a single line to the output signal frequency of each LED lamp. The optical transducer (CMOS photo-detector), which converted light into an electrical quantity, was chosen to collect the light intensity transmitted through the optical gas sensor. This photo-detector was the color light-to-frequency converter module (TCS230) from Texas Advanced Optoelectronic Solutions Company (Plano, TX, USA). The output data was constructed as a square wave with frequency directly proportional to light intensity. Wavelengths corresponding to red, yellow, green, pink, blue, and violet LEDs were centered at 638, 587, 537, 472, 457, and 399 nm, respectively, while white and infrared LEDs represented the broad spectrum light around 450–700 and 700–1 × 10^6 nm, respectively. The intensity

of light transmitted through the optical gas sensor was detected from the photon frequency (Hz) that interacted directly with the photo-detector during the dynamic gas flow measurement, see Figure 2b. An array of optical gas sensors was generated with LED lights of eight colors (infrared, red, yellow, green, violet, pink, blue, and white). N_2 was used as the pure carrier (reference) gas, delivering odors to the sensor chamber. The flow rate of the N_2 gas was controlled by a mass flow meter at a constant rate of 700 mL/min. Measurement of the dynamic gas flow system was performed by switching between the sample gases for 2 min and the N_2 for 2 min. This process was repeated for 5 cycles. The gas sensing response (S) from the eight sensors was the difference between the maximum peak (signal frequency from the sample odor) and the baseline (signal frequency from the reference gas). These responses were used as the input data for pattern recognition by principal component analysis (PCA). The gas sensing response (S) was defined as the light intensity change in the frequency during the presence of dynamic gas flow measurements as follows (equation (2)):

$$S = \left(\frac{f_S - f_R}{f_R} \right) \times 100 = \frac{\Delta f}{f_R} \times 100 \quad (2)$$

where f_R is the initial frequency of each optical wavelength without the sample vapor (baseline frequency) and f_S is the frequency when exposed to the testing gas vapor, see in Figure 2b. The gas sensing response (S) can be calculated from a differential comparison between the initial frequency of each optical wavelength (baseline frequency or f_R) and the frequency when exposed to the testing gas vapor (f_S). Therefore, spectral sensitivity can be represented as a percentage of the changes in the frequency signal relative to the initial frequency of each optical wavelength.

3.3.2 Nanocomposite gas sensor based on organic-inorganic dyes and carbon nanotube

Fabrication of organic-inorganic nanocomposite gas sensors

Organic and inorganic dyes, namely, zinc-2,9,16,23-tetra-tert-butyl-29H,31H-phthalocyanine (ZnTTBPc), zinc-5,10,15,20-tetra-phenyl-21H,23H-porphyrin (ZnTPP) and cobalt-5,10,15,20-Tetraphenyl-21H,23H-porphine (CoTPP) were obtained from Sigma-Aldrich whereas multiwall carbon nanotubes (MWCNTs) was obtained from Chiang Mai University (synthesized by Dr. Phisit Singjai). Firstly, ZnTTBPc, ZnTPP and CoTPP were dissolved in chloroform solution at the concentration of 5 mg/ml while MWCNT was dissolved in chloroform solution at the concentration of 2 mg/ml. Next, the solutions of MWCNT was mixed in the dye solution of (i) ZnTTBPc, (ii) ZnTPP and (iii) CoTPP in the

ratio 1:1 (volume: volume). The molecular structure of ZnTTBPc, ZnTPP and CoTPP were shown in Figure 3(a). Finally, three composite gas sensors (i.e. ZnTTBPc/MWCNT, ZnTPP/MWCNT and CoTPP/MWCNT) were prepared by spinning the mixed solution onto the interdigitated Cr/Au electrode substrates for the electrical measurement (see Figure 3(b)). This interdigitated electrode was fabricated by evaporation process of Cr/Au over alumina substrates. The thickness of Cr and Au layers were about 50 nm and 200 nm, respectively. Furthermore, the resistance change (kΩ) of these gas sensors upon contact with the VOC vapor at room temperature were recorded by the voltage divider circuit.

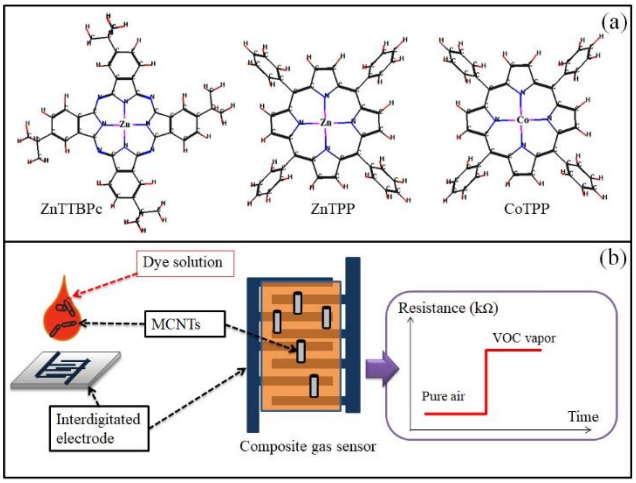

Figure 3 (a) Structures of ZnTTBPc, ZnTPP and CoTPP molecules and (b) the preparation process of organic-inorganic dyes/multiwall carbon nanotubes (MCNTs) composite gas sensor on the Cr/Au interdigitated electrode.

Metal-oxide semiconductor (MOS) gas sensors

The commercial MOS gas sensors, namely, TGS 2444, TGS2603 and TGS 2620 were obtained from Figaro USA Inc. company. The sensing layer of these sensors were metal oxide semiconductor (MOS) such as SnO_2 and WO. These layers were formed on an alumina substrate of a sensing chip together with an integrated heater. Thus, after applying heating voltage, the sensing layer reacted with oxidizing or reducing gases. Then the resistance of this layer changed due to the increasing or decreasing of the targeted VOC concentration.

Performance of the hybrid gas sensor arrays

The details of gas sensor arrays in hybrid e-nose are listed in Table2. TGS 2444 has a high selective for ammonia gas and some response to hydrogen sulfide. TGS2603 sensitives to low concentrations of amine-series and sulfurous vapors such as trimethyl

amine, hydrogen sulfide, hydrogen and ethanol. TGS 2620 has a high selective for the general organic solvents, for example, alcohol, carbon monoxide and hydrogen. In addition, nanocomposite gas sensors, namely, ZnTTBPc/MWCNT, ZnTPP/MWCNT and CoTPP/MWCNT were used as the general organic solvent detection such as alcohol, acetone, acetic acid, etc.

Table 2 Property of the gas sensors in the hybrid e-nose system

Sensor No.	**Sensor class**	**Sensor details** (detected compounds)	**Typical detection range (**ppm**)**
S1	ZnTTBPc/MWCNT	Nanocomposites gas sensor (organic solvents)	>902*
S2	ZnTPP/MWCNT	Nanocomposites gas sensor (organic solvents)	>515*
S3	CoTPP/MWCNT	Nanocomposites gas sensor (organic solvents)	>2,433*
S4	TGS 2444	MOS (ammonia and hydrogen sulfide)	>166*, 10-300**
S5	TGS2603	MOS (amine-series and sulfurous vapors)	>236*, 1-10**
S6	TGS 2620	MOS (alcohol and organic solvents)	>141*, 50-5,000**

* Typical detection range was calculated from the experiment.

** Typical detection range was reported from manufacturer (Figaro).

In this experiment, the sensitivity and selectivity of gas sensors were tested with acetic acid, acetone, ammonia, ethanol, ethyl acetate, formaldehyde and H_2O which were reported as the most general VOC that generated during bacterial culture process. The detail of VOC preparation is shown in Table 3. Each VOC was evaporated at the different temperature which is related to their boiling point. Moreover, VOC volume in cylinder was calculated based on their density. Thus, VOC solution was injected to the 1,000 mL bottle which is in the heated bath for temperature control. Then, 400 mL min^{-1} of pure air (air zero) was used as the carrier gas in this system. Finally, resistance change of each gas sensor was measured by hybrid e-nose system.

Table 3 Preparation of VOCs at the concentration of 1,000 ppm in pure air.

VOCs	Evaporated temperature* (°c)	M.W. ($g\ mol^{-1}$)	Density ($g\ mL^{-1}$)	Volume of VOC in cylinder (μL)
Acetic acid (35%)	100	60.05	1.05	2.60
Acetone (100%)	56	58.08	0.79	3.29
Ammonia (29%)	25	17.03	0.91	0.84
Ethanol (100%)	78	46.07	0.79	2.62
Ethyl acetate (100%)	77	88.11	0.90	4.38
Formaldehyde (37%)	25	30.03	1.09	1.24
H_2O (100%)	100	18.02	1.00	0.81

*Evaporated temperature is depended on the boiling point of each VOC.

The sensor response from six gas sensors describes the sensitivity of gas sensor. The percentage of sensor response (%sensitivity) is defined as the following equation:

$$\%\text{sensitivity} = \frac{\Delta R}{R_0} \times 100 \quad (3)$$

where R_0 is the resistance value of a gas sensor in pure air and ΔR is the different resistance value between sample and pure air.

3.4 To apply the e-nose system for the bacterial identification

The growing media for bacteria in this work is lysogeny broth or LB media. This media is prepared by dissolving tryptone (10g), yeast extract (5g) and NaCl (5g) in deionized water (1L). Then pH of solution will be adjusted in the range of 7.2-7.4 by using NaOH. Single bacterial colony from LB agar plate is added to the 5 ml of LB tube. Incubate bacterial culture at 37°C for 9hr in a shaking incubator (180 rpm). After incubation, check for bacterial growth, which is characterized by a cloudy media.

Next, the concentration of initial bacteria will be controlled by measuring the optical density (OD) of LB solution. OD of solution is measured by UV-Visible spectrophotometer at wavelength 600 nm in absorption mode. OD of LB media is controlled by adding the H_2O until the OD equal to 0.3. Then the 25 µl of adjusted LB is added to 25 ml of pure LB. Then the OD and the vapor of culture bacterial solution will be collected.

The optimized condition (i.e. temperature, gas flow rate, time of sampling, etc.) for bacterial identification will be investigated. Finally, pattern recognition will be classified 5 types of pathogenic bacteria, namely, *E. cloacae, E. coli, P. aeruginosa, S. aureus* and *S. Typhi.* Firstly, gram-negative bacteria (*E. cloacae, E. coli, P. aeruginosa and S. Typhi*) and gram-positive bacteria (*S. aureus*) will be separated by e-nose. Finally, 4 types of gram-negative bacteria, namely, *E. cloacae, E. coli, P. aeruginosa and S. Typhi* will be identified.

4. Results and discussion

4.1 To study the interaction energies and electronic properties between organic-inorganic dyes and VOCs molecule using density functional theory calculation (DFT)

The interaction energy between organic-inorganic molecule and VOC are reported in Figure 4.

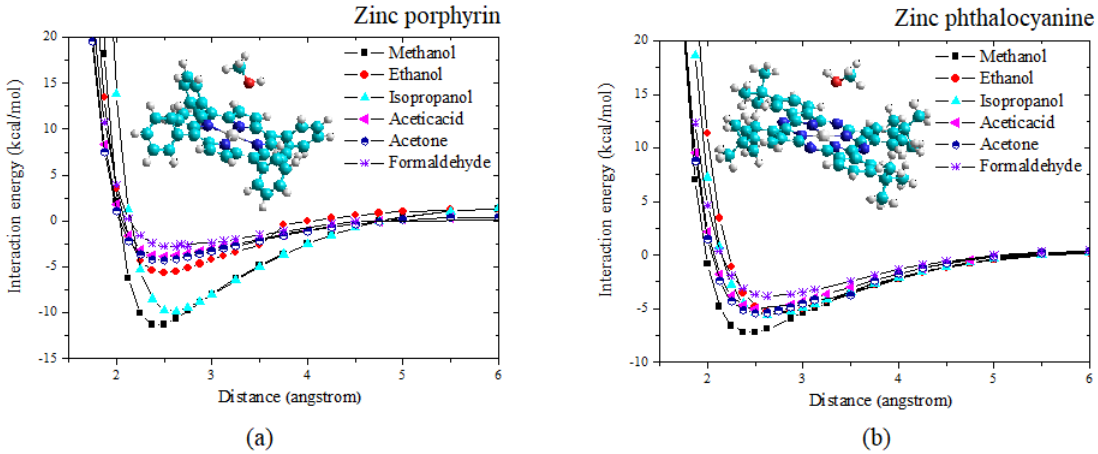

Figure 4. The interaction energy between VOC molecule and (a) Zinc-porphyrin and (b) Zinc-phthalocyanine.

The highest interaction energy of both sensing molecules were observed with about 2-3 Å for both Zinc-porphyrin and Zinc-phthalocyanine. Both compounds presented the highest interaction energy with methanol. Moreover, other VOCs presented ability to bind with both sensing molecules. This calculation result indicates that porphyrin and phthalocyanine had a potential to interact with VOC.

4.2 Develop the hybrid gas sensor platform for nanocomposite gas sensor and metal oxide semiconductor gas sensors in e-nose setup

The constructed briefcase hybrid E-nose system is shown in Figure 5. This system involves four main elements: sensor chamber, controller circuit, odor delivery sections and data acquisition (DAQ). In this work, there were 2 types of gas sensor, i.e. MOS and nanocomposite gas sensors. Six gas sensors were placed in sensor chamber which is made from Teflon material. The controller circuit provided current for both MOS and nanocomposite gas sensors. For the odor delivery sections, the sample bottle was the commercial glasses (100 ml Schott, Duran) with polypropylene screw caps and pouring rings.

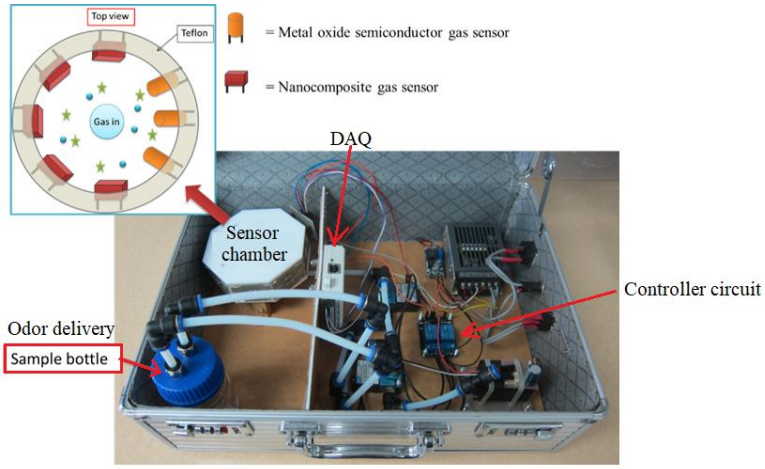

Figure 5. Constructed briefcase of the hybrid gas sensor platform.

4.3 To develop the gas sensor based on organic- inorganic dyes and carbon nanotube for the specific VOCs in bacterial growing phase

4.3.1 Optical gas sensor

In this work, the optical gas sensor was fabricated by employing metal free organic- inorganic dyes, namely ZnTPP, ZnTTBPc and MnTPPCl. Effect of thermal treatment on structure and the sensitivity property of optical gas sensor was investigated by UV-Vis spectroscopy.

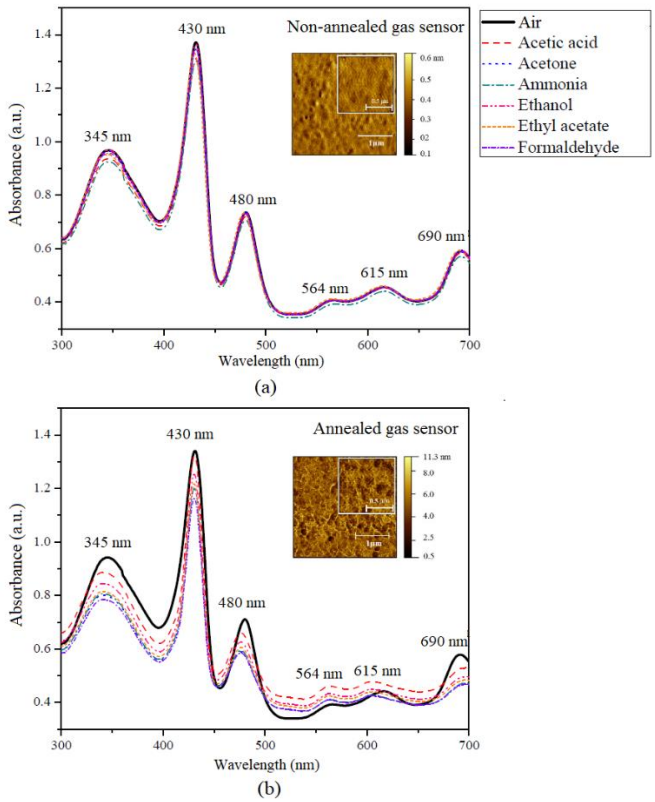

Figure 6. AFM image and UV-Visible absorption spectra change of (a) non-treated and (b) thermally treated gas sensors under VOCs atmosphere.

Figure 6 shows the changes in the absorption spectrum of optical gas sensors in the case of thermal treatment and without thermal treatment. Six volatile compounds (10% in aqua) such as acetic acid, acetone, ammonia, ethanol, ethyl acetate and formaldehyde were selected for the sensor performance testing. In the case of non-treated gas sensor, the maximum absorption of this sensor centered at 345, 430, 480, 564, 615 and 690 nm (see in Figure 6(a)). The Soret bands of the ZnTTBPc, ZnTPP and MnTPPCl are the absorption peaks at 345, 430 and 480 nm, respectively. These absorption bands that can be observed in the 400-500 nm range are related to n-π* transitions of the lone nitrogen pair orbital of the macrocycle. The peak at 564 nm and 615 nm are the Q bands of porphyrin compound, while the peak at 690 nm is the Q band of the ZnTTBPc. These Q bands are related to the π-π* transitions of the porphyrin macrocycle ring. The shift of the absorption spectrum in both cases (with and without thermal treatment process) of gas sensors when exposed to VOCs vapors were observed near each main peak of both gas sensors namely 345, 430, 480, and 690 nm (see in Figure 6(a)-(b)). These absorption spectral shifts of gas sensor related to the electron interchange between the analyte gas and π-π conjugated system of porphyrin molecule that effected to the electron density for π-π* transitions. The results show that the absorption spectra change of thermal treated gas sensor has much-stronger changes in absorption than non-treated gas sensor, especially at 345, 430, 480 nm. Therefore, the absorption spectra change at the Q band and B band of gas sensor was deeply calculated. The surface morphology of non-treated and treated gas sensors were characterized by using AFM as shown in Figure 6. Surface roughness of thin films gas sensors in case of non-thermal treated film and thermal treated film are 0.494 nm and 0.961 nm, respectively. Thus, thermal treatment process can promote additional changes from the smooth surface to a knobbed surface.

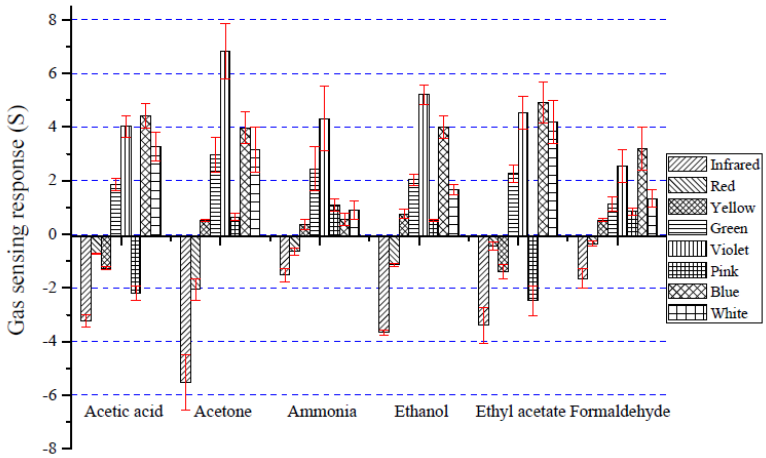

Figure 7. The gas sensing response (S) of thermally treated gas sensors toward 10% (volume/volume) of VOCs in aqua under dynamic gas flow conditions.

Figure 7 shows a comparison of the gas sensing response (S) of the thermally treated gas sensor when exposures to different VOCs (10% in aqua) under dynamic gas flow conditions. An in-house optical artificial nose was used to study the performance of thin-film sensing materials. The gas sensing response (S) was calculated from the light intensity change between the signal on light intensity of sensor without the sample vapor (baseline light intensity, f_R) and the signal when exposed to the testing gas vapor (f_S) (see Equation (2). The array of eight optical gas sensor were generated from the different LED light sources such as infrared, red, yellow, green, violet, pink, blue and white LEDs. The sensitivity of gas sensor depends on the different LED light sources and the different types of VOCs. The sensing signal from the yellow, green, violet, blue, and white LEDs show the positive values of sensitivity, while the infrared, red, yellow and pink LEDs show the negative value of sensitivity. These results show that the light intensity was changed during the sensors are placed in the vapor flow of the sampling system. The excellent sensitivity behavior was found in the case of the violet, blue, infrared and white LED for all VOCs, which demonstrate that the most active site for sensing signals were observed at 399 nm, 457 nm, infrared region and broad spectrum light. The highest sensitivity to the gas was found in the acetone vapor at the violet LED. The gas sensor has distinct response patterns with different gas, which these VOCs were used to represent the odors that release from bacterial growth. Therefore, the thermally treated gas sensor was proposed for bacterial identification.

4.3.2 Nanocomposite gas sensor based on organic-inorganic dyes and carbon nanotube

In order to evaluate the performance of nanocomposite gas sensor, seven VOCs such as acetic acid, acetone, ammonia, ethanol, ethyl acetate formaldehyde and H_2O were selected to test at the concentration of 1,000 ppm.

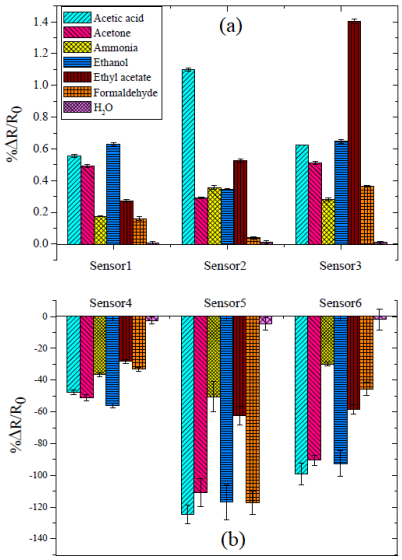

Figure 8 Average of %sensitivity for *(a)* nanocomposite gas sensor and *(b)* MOS gas sensor toward VOCs at the concentration of 1,000 ppm under dynamic gas flow conditions *(*400 ml min^{-1}*)*.

Figure 8 shows the %sensitivity (see equation (3)) of three nanocomposite gas sensors and three MOS gas sensors under dynamic gas flow in hybrid e-nose system. The %sensitivity for nanocomposite gas sensors and MOS gas sensors were found in the range 0.002-1.405 and 1.858-99.028, respectively. However, MOS gas sensor provided greater sensitive than nanocomposite gas sensors, both types of gas sensor presented the different pattern depend on VOC type.

In case of nanocomposite gas sensors, Sensor3 (CoTPP/MWCNT) provided highest % sensitivity for ethyl acetate vapor when compared to Sensor1 (ZnTTBPc/MWCNT) and Sensor2 (ZnTPP/MWCNT). All nanocomposite gas sensor presented specific pattern of %sensitivity, for example, Sensor1 and Sensor2 provided high %sensitivity to ethanol and acetic acid, respectively. Moreover, all sensors presented low %sensitivity for H_2O. It means that all nanocomposite gas sensor which were fabricated from porphyrin and phthalocyanine had high ability to use as the general VOC detection.

In case of MOS gas sensors, Sensor5 provided high %sensitivity for acetic acid, ethanol and formaldehyde when compared to Sensor4 and Sensor6. Sensor6 presented excellent %sensitivity to acetic acid, acetone and ethanol. In contrast, Sensor4 presented poor %sensitivity for all VOCs. Based on current results, Sensor5 had high ability to use as gas sensor; however, Sensor1, Sensor2, Sensor3, Sensor4 and Sensor6 which presented the particular pattern of %sensitivity were necessary for VOC classification in

e-nose technique because the efficiency of e-nose system can be improved using several types of gas sensor.

4 To apply the hybrid e-nose system for the bacteria identification

Single bacteria colony from LB agar plate is added to the 5 ml of LB tube. Incubate bacterial culture at 37°C for 9hr in a shaking incubator (180 rpm). The concentration of initial bacteria LB media will be controlled by measuring the optical density (OD) at 600 nm. Then, the growth curve of each bacterial strain in liquid media was investigated every 3 hours as shown in Figure 9.

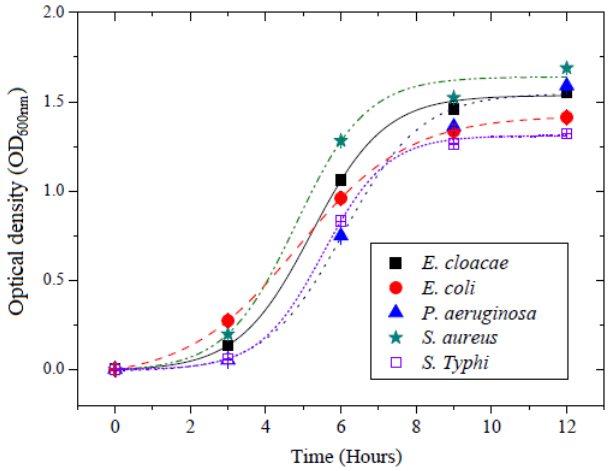

Figure 9. The optical densities of *E. cloacae, E. coli, P. aeruginosa, S. aureus* and *S. Typhi* in culture media performed in triplicates and the error bars represent standard deviations. Black square, red circle, blue triangle, green star and violet square represent the data points used to construct the growth curves of *E. cloacae, E. coli, P. aeruginosa, S. aureus* and *S. Typhi*, with R-squared (R^2) statistics of 0.99857, 0.99998, 0.99003, 0.99415 and 0.99929, respectively.

To start an experiment, the flow rate of pure air was controlled at 400 mL min^{-1}. The temperature of sample bottle was controlled 37 ºC for bacterial sample and evaporated temperature for VOC sample. The absorption of this media was investigated (in triplicate) at the wavelength of 600 nm. The growth phase was observed during the 12-h of incubation. The growth curves of bacteria were plotted by polynomial equation i.e. $Y = A_1 + (A_2-A_1)(1+10^{((\mathrm{Log}X_0-X)*P)})^{-1}$, whereas, X is time, Y is optical density and A_1, A_2 and P are the constant value. The coefficient of determination (R-squared) of *E. cloacae*, *E. coli*, *P. aeruginosa*, *S. aureus* and *S. Typhi* fitted curves were reported as 0.99857, 0.99998, 0.99003, 0.99415 and 0.99929, respectively. The initial cell concentration was

controlled by used the same value of OD_{600nm}. Based on the fitted curve, the cell density of all bacteria slightly increased after 3 hour of incubation and rapidly increased during 3-9 hour of incubation. The stationary phase (no further increase in the cell density) of all five bacterial strains was observed after 9 hour of incubation. All bacteria were observed to have a similar growth pattern; however, *S. aures* and *E. cloacae* enter the log phase quicker than *E. coli*, *S. Typhi* and *P. aeruginosa* which displayed a prolonged lag period. It means that each bacteria present the unique growth behavior that should relate to the VOC releasing.

In this work, bacterial identification was investigated by 2 systems of e-nose, namely, optical and electrical e-nose systems as follow.

4.1 Optical e-nose system

Optical e-nose was applied for bacterial classification based on optical gas sensor. The gas sensing signal of gas sensor was investigated by measuring the optical property change under gas flow system.

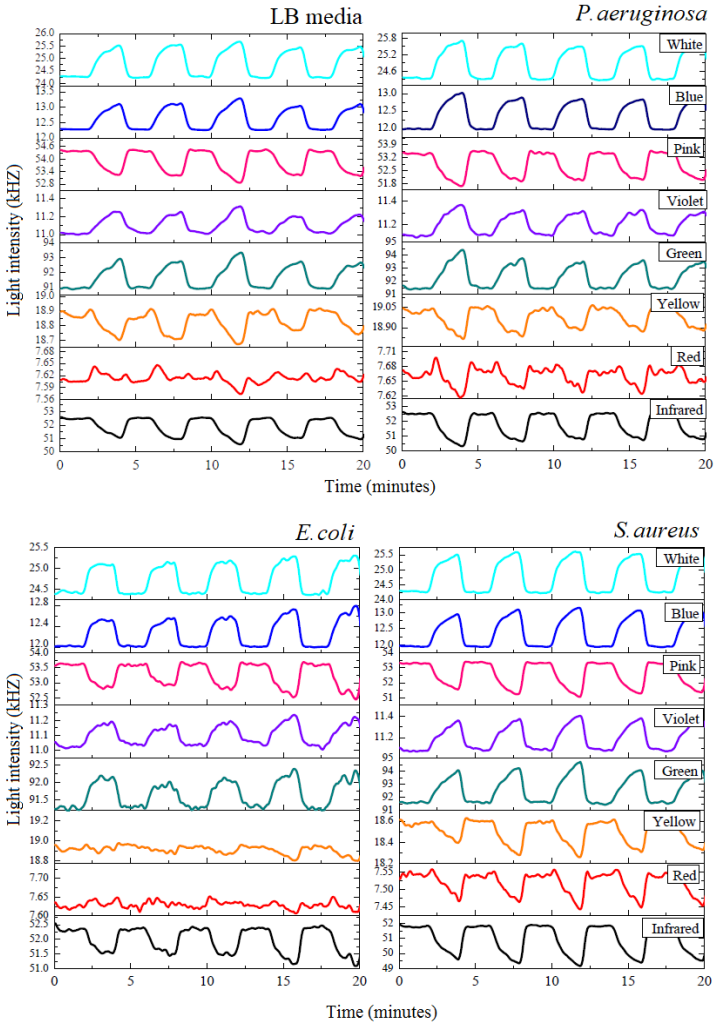

Figure 10. The gas sensing signal of the thermally treated gas sensor with LB media and three types of bacteria under the in-house optical artificial nose measurement.

The optical gas sensor was used to detect malodorous volatiles are produced by three pathogenic bacteria and LB media odor. Figure 10 illustrates the examples of the optical gas sensor array signal from bacteria growing over a 9 hours of incubation period. Nitrogen gas was used as the reference gas to deliver fresh air to clean the chamber and also used as carrier gas to deliver the gas samples of interest to the sensor chamber. While conducting the measurement, the LB media sample was controlled temperature of about 37°C. The sensorgram shows the level of light intensity signal obtained from analysis of optical sensor array that consists of eight channel of gas sensors generated from the eight LED light sources, namely infrared, red, yellow, green, blue, pink, violet and white LED.

The increasing of optical sensing signals was found at the green, blue, violet and white LEDs, while the decreasing of optical sensor signals were found at the infrared, red, yellow and pink LEDs. The optical sensing signal of *P. aeruginosa* and *S. aureus* was found prominently displayed in the entire LED light sources but *E. coli* could not be observed in red and yellow LEDs. Therefore, the optical sensing signal patterns of *P. aeruginosa* and *S. aureus* were different from *E. coli.* Even through the optical sensing signal patterns of *P. aeruginosa* is similar to *S. aureus* the variations of optical sensing signal path are different. Thus, optical gas sensors have a great potential to detect and classify the three types of pathogenic bacteria based on sensing signal patterns analysis.

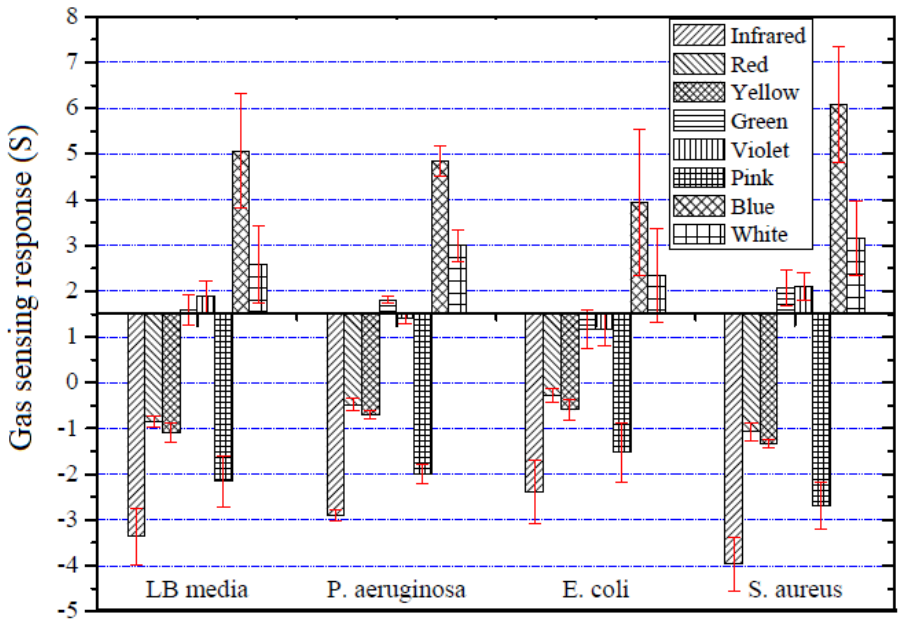

Figure 11. The gas sensing response (S) of the thermally treated optical gas sensors toward three types of bacteria in culture media after 9 hours of incubation.

To evaluate the optical gas sensor potential for bacterial identification, the optical gas sensor was exposed to VOCs in three bacteria: *P. aeruginosa*, *S. aureus* and *E. coli* as show in Figure 11. The average of percent change in the light intensity of optical sensors under the dynamic measurement system when exposed to volatile samples were calculated according to Equation *(2)*. The results indicate that not only blue LED shows the highest sensing response for three different types of bacteria, but also show that the bacteria produce a wide range of VOCs with different pattern of bacteria growth. These sensing responses of optical gas sensors are related to the amount of VOCs and the types of compounds that emitted from bacterial activity.

The optical gas sensor is exposed to the smell of bacteria growing, which causes changes in its output signal until the sensor reaches steady state. Three major physical features, including min-max values, slope values and integral area values were selected for feature extraction technique based on the analysis of the covariance between the factors. Principal component analysis (PCA) is suitable for the multi-dimensional datasets of this work where data are collected from eight optical sensors array and multiple odors. The complex data set (multiple dimensions) was transformed using the matrix that represented general values in the form of new data set (2 or 3 dimensions). Then, the PCA result was obtained by matrix multiplication and transpose. The PCA results in this work were presented in the form of its new principal components (PC). First principal component (PC1) was contained most variance of data set than other component (i.e. PC2 and PC3).

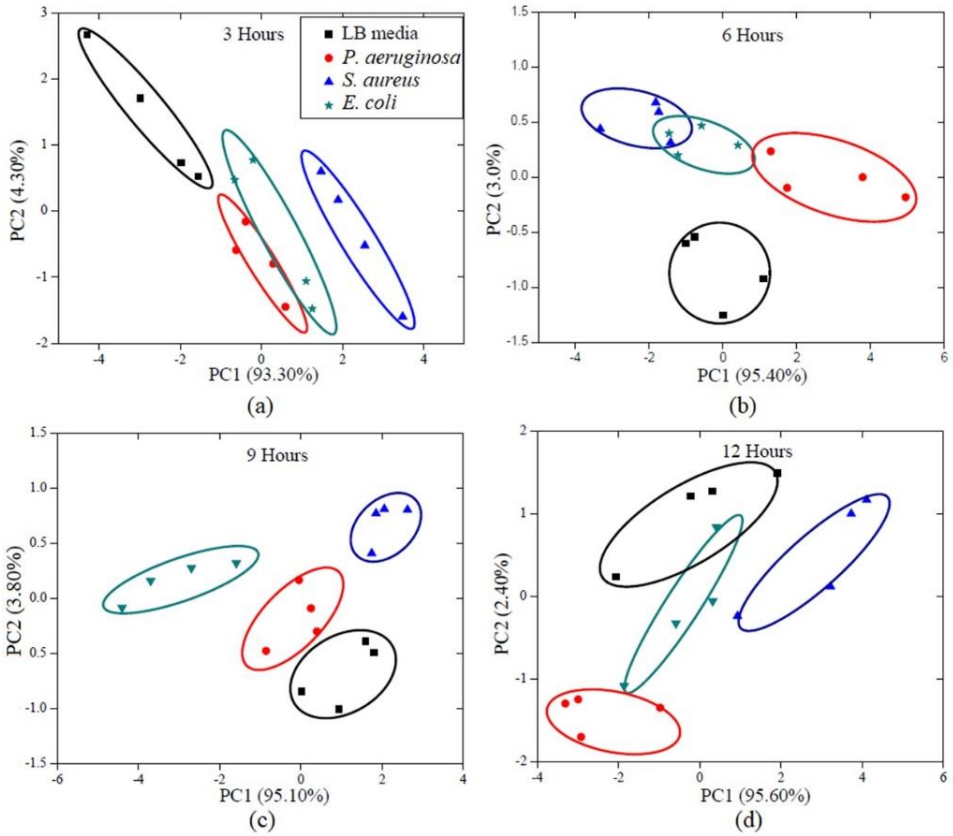

Figure 12. Schematic diagram of PCA of three types of pathogenic bacteria in mediums under in-house artificial nose measurement.

Figure 12 shows the identification of three types of pathogenic bacteria and LB media in PCA plots. Effect of incubation period on growth and bacteria activity, that a change in smell was investigated every 3 hours. It was found that the pure LB media, *P. aeruginosa*, *S. aureus* and *E. coli* can be distinguished and grouped using the eclipses within 95% confidence. Figure 12(a)-(c) shows the distinct clusters of pure LB media and three bacteria samples, which are separated into four groups within 3- 12 hours of incubation period. After 9 hours of incubation times, Figure 12*(c)* shows the best discrimination performance between the different types of bacteria and LB media sample. PC1 accounts for the greatest variance (95.10%). Thus, it was found that the four data clusters are clearly separated on the PC2 axis, while the data points of the bacteria odors and LB media are scattered along the PC1 axis.

4.2 Hybrid e-nose system

Hybrid e- nose was applied for bacterial classification based on MOS and nanocomposite gas sensors. The gas sensing signal was investigated by measuring the electrical property change under gas flow system.

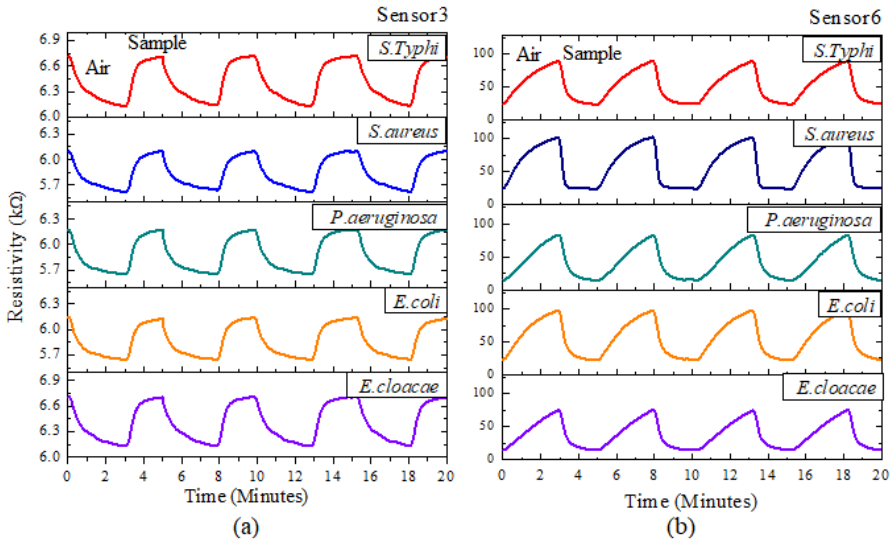

Figure 13. A signal of the (a) Sensor 3 (CoTPP/MWCNT) and (b) Sensor 6 (TGS2620) recorded as resistance values versus time for bacterial growing at 6 hours.

Figure 13 shows the example of sensing signal for nanocomposite gas sensor (CoTPP/MWCNT) and MOS gas sensor (TGS2620) toward the culture bacterial odor. The resistance signal of gas sensor was recorded as a function of time. Each experiment was repeated 4 times. The experiment started by flowing reference gas (pure air) to for 3 minutes and then switching to bacterial odor for 2 minutes. The resistance values of nanocomposite gas sensor increased after switching to bacterial odor (Figure 13(a)) while the resistance values of MOS gas sensor decreased after switching to bacterial odor (Figure 13(b)). Moreover, the resistance of nanocomposite gas sensor rapidly increases within 41 seconds and the resistance of MOS gas sensor gradually decreases within 45 seconds.

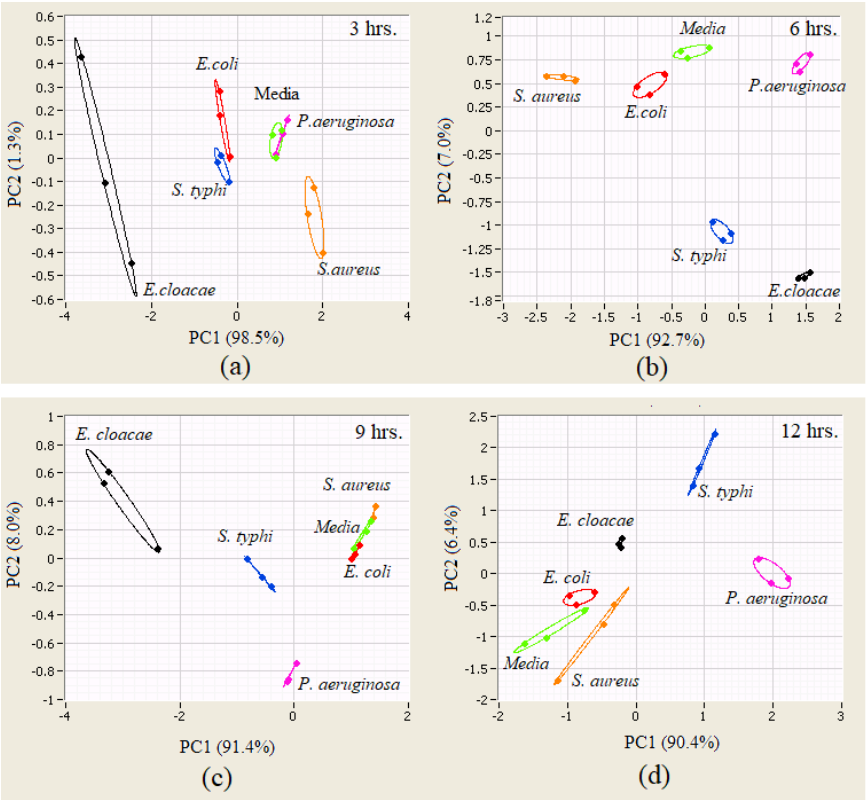

Figure 14 Schematic diagram of PCA of five types of pathogenic bacteria in mediums by varying incubation time based on hybrid e-nose system.

Figure 14 shows the identification of five pathogenic bacteria and LB media in PCA plots. Effect of incubation period on growth and bacteria activity, that a change in smell was investigated every 3 hours. It was found that the pure LB media, *E. cloacae*, *E. coli, P. aeruginosa, S. Typhi* and *S. aureus* can be distinguished and grouped using the eclipses within 95% confidence. Figure 14(a)-(d) shows the distinct clusters of pure LB media and five bacteria samples. After 6 hours of incubation times, Figure 14(b) shows the clear discrimination performance between the different types of bacteria and LB media sample. PC1 accounts for the greatest variance (92.7%). Moreover, after 12 hours of incubation times, this e-nose system presents the clear discrimination performance again (see in Figure 14(d)).

It can be found that the incubation time at 6 hours shows the clear separation of three bacteria sample and has an individual unique pattern of odor (Smell fingerprint), as their odor differed not only in each species, but also differs with the scent of the culture medium. These findings will pave the way for further development of specifically designed gas sensor system for bacteria odor detection which is very sensitive to different odors from bacterial samples.

5. Conclusion

In this work, two types of gas sensor e.g. optical gas sensor and nanocomposite gas sensor were developed using organic-inorganic dyes such as metallo-porphyrin and metallo-phthalocyanine. Moreover, optical e-nose system and electrical e-nose system were proposed to predict the pathogenic bacterial species based on the volatile organic compound (VOC) from bacteria in culture medium as follow:

For optical e-nose system, the sensitivity and stability of optical gas sensors were enhanced by the thermal treatment process. The in-house optical artificial nose system based on light emitting diode and photo detector was successful to investigate the characteristic of a new optical gas sensor under the dynamic gas flow system. The identification of bacteria was successfully detected by the PCA within the incubation time of 9 hours. The results showed the feasibility of using this in-house optical artificial nose system for real time discrimination of bacteria odor to indicate the different bacteria species and phases of bacterial growth. The capability to detect various VOCs as related to the bacteria growing, especially acetic acid, acetone, ammonia, ethanol, ethyl acetate and formaldehyde have been demonstrated. Based on pattern recognition techniques for odor discrimination in optical gas sensor arrays, we have shown that the proposed optical sensing material combined artificial nose system can discriminate the odor of three bacteria species for the non-invasive pathogenic bacteria monitoring.

For electrical e-nose system, this system was developed from the nanocomposite gas sensors and MOS gas sensors. The capability of this system was tested by specific VOCs from bacteria, especially acetic acid, acetone, ammonia, ethanol, ethyl acetate, and formaldehyde. The nanocomposite gas sensors (sensor1, sensor2, and sensor3) and MOS gas sensors (sensor4, sensor5, and sensor6) represented the different pattern of % sensitivity based on the targeted gas. The discrimination of five groups of bacteria was presented by PCA analysis at the variation of 99.70% within the 6 hours of incubation period. It indicates that this e-nose system has a potential to apply for bacterial screening test.

Output จากโครงการวิจัยที่ได้รับทุนจาก สกว.

1. ผลงานตีพิมพ์ในวารสารวิชาการนานาชาติ (ระบุชื่อผู้แต่ง ชื่อเรื่อง ชื่อวารสาร ปี เล่มที่ เลขที่ และหน้า) หรือผลงานตามที่คาดไว้ในสัญญาโครงการ

   1. 1 **Sumana Kladsomboon**, Chadinee Thippakorn, Thara Seesaard* Development of organic- inorganic hybrid optical gas sensors for the non-invasive monitoring of pathogenic bacteria. Sensors (Switzerland) . 2018;18(10).

   1.2 Thara Seesaard, Chadinee Thippakorn, Teerakiat Kerdcharoen, **Sumana Kladsomboon*** A hybrid electronic nose system for discrimination of pathogenic bacterial volatile compounds. Analytical Methods. 2020; DOI: 10.1039/D0AY01255F.

2. การนำผลงานวิจัยไปใช้ประโยชน์
   - เชิงวิชาการ พัฒนาศักยภาพนักศึกษาในด้านการวิจัยโดยคณะเทคนิคการแพทย์ มหาวิทยาลัยมหิดล ดังนี้
     - นางสาวนภเนตร เรือนเย็น นักศึกษาหลักสูตรปริญญาวิทยาศาสตรบัณฑิต (เทคนิคการแพทย์) คณะเทคนิคการแพทย์ มหาวิทยาลัยมหิดล หัวข้อภาคนิพนธ์ “Development of hybrid gas sensor system for pathogenic bacterial analysis”
     - นางสาวภัทรวดี คำม่วง นักศึกษาหลักสูตรปริญญาวิทยาศาสตรบัณฑิต (เทคนิคการแพทย์) คณะเทคนิคการแพทย์ มหาวิทยาลัยมหิดล หัวข้อภาคนิพนธ์ “Development of chemical gas sensor for healthcare and safety applications”
     -

3. อื่นๆ (เช่น ผลงานตีพิมพ์ในวารสารวิชาการในประเทศ การเสนอผลงานในที่ประชุมวิชาการ หนังสือ การจดสิทธิบัตร)

   - “Optical gas sensor based on porphyrin and phthalocyanine compounds for pathogenic bacterial identification” ในการประชุม 5th International Conference on Bio-Sensing Technology, 2017, Riva Del Garda, Italy. (Poster presentation)

รายงานสรุปการนำผลงานวิจัยไปใช้ประโยชน์

สัญญาเลขที่ MRG6080151 **ชื่อโครงการ** จมูกอิเล็กทรอนิกส์แบบไฮบริดที่พัฒนาจากก๊าซเซ็นเซอร์แบบโลหะออกไซด์ร่วมกับก๊าซเซ็นเซอร์แบบนาโนคอมโพสิตเพื่อใช้ในการระบุชนิดของแบคทีเรีย
หัวหน้าโครงการ....ผู้ช่วยศาสตราจารย์ดร. สุมนา กลัดสมบูรณ์....**หน่วยงาน**..คณะเทคนิคการแพทย์ มหาวิทยาลัยมหิดล..
โทรศัพท์.....0891194147.....**โทรสาร**.....**อีเมล์**.....sumana.kla@mahidol.edu.....
สถานะผลงาน √ ปกปิด □ ไม่ปกปิด

ความสำคัญ / ความเป็นมา

Bacterial infection is commonly occurred in the skin and soft tissue for the human. Even though most pathogenic bacteria such as *E. cloacae, E. coli, P. aeruginosa, S. aureus* and *S. Typhi.* can be found in the environment, current technique for bacterial identification, i.e., cell culture method, time at least 24-48 hours and needs specialist to identify. Previous studies found that the pattern of volatile organic compounds (VOCs) which were produced during the bacterial culture period depended on the bacterial species. Moreover, each bacteria species produced specific VOCs profile and generated the unique growth curve. Therefore, the idea to identify bacteria based on VOCs profile was studied. At the first period of this research, gas chromatography–mass spectrometry (GC-MS) which is the standard technique was applied to identify the VOCs. However, GC-MS was complicated technique for user and had high-cost for patient. Therefore, the alternative method, namely, electronic nose (e-nose) was proposed for the label-free and non-invasive method in real time analysis. This e-nose technique comprised gas sensor arrays and pattern recognitions. Gas sensor arrays are applied for the volatile organic compound (VOC) detection while pattern recognitions are applied for the data analysis. To increase the e-nose performance, gas sensors arrays for specific VOCs need to be developed.

วัตถุประสงค์ของโครงการ

1 To study the interaction energies and electronic properties between organic-inorganic dyes and VOCs molecule using density functional theory calculation (DFT)

2 To develop the hybrid gas sensor platform for nanocomposite gas sensor and metal oxide semiconductor gas sensors in e-nose setup

3 To develop the gas sensor based on organic-inorganic dyes and carbon nanotube for VOCs detection

4 To apply the e-nose system for the bacterial identification

ผลการวิจัย (สั้น ๆ ที่บ่งชี้ประเด็นข้อค้นพบ กระบวนการ ผลผลิต และการเรียนรู้)

In this work, two type of gas sensor e.g. optical gas sensor and nanocomposite gas sensor was developed based on organic-inorganic dyes such as porphyrin and phthalocyanine. Moreover, optical e-nose system and electrical e-nose system were proposed to predict the pathogenic bacterial species based on the volatile organic compound (VOC) from bacteria in culture medium as follow:

For optical e-nose system, the sensitivity and stability of optical gas sensors were enhanced by the thermal treatment process. The in-house optical artificial nose system based on light emitting diode and photo detector was successful to investigate the characteristic of a new optical gas sensor under the dynamic gas flow system. The identification of bacteria was successfully detected by the PCA within the incubation time of 9 hours. The results showed the feasibility

of using this in-house optical artificial nose system for real time discrimination of bacteria odor to indicate the different bacteria species and phases of bacterial growth. The capability to detect various VOCs as related to the bacteria growing, especially acetic acid, acetone, ammonia, ethanol, ethyl acetate and formaldehyde have been demonstrated. Based on pattern recognition techniques for odor discrimination in optical gas sensor arrays, we have shown that the proposed optical sensing material combined artificial nose system can discriminate the odor of three bacteria species for the non-invasive pathogenic bacteria monitoring.

For electrical e-nose system, this system was developed from the hybrid gas sensor platform for nanocomposite gas sensors and MOS gas sensors. The capability of this system was tested by specific VOCs from bacteria, especially acetic acid, acetone, ammonia, ethanol, ethyl acetate, and formaldehyde. The nanocomposite gas sensors (sensor1, sensor2, and sensor3) and MOS gas sensors (sensor4, sensor5, and sensor6) represented the different pattern of %sensitivity based on the targeted gas. The discrimination of five groups of bacteria was presented by PCA analysis at the variation of 99.70% within the 6 hours of incubation period. It indicates that this e-nose system has a potential to apply for bacterial screening test.

คำสืบค้น (Keywords)
electronic nose; porphyrin; phthalocyanine; pattern recognition; bacterial discrimination

การนำผลงานวิจัยไปใช้ประโยชน์ (ดูคำจำกัดความ และตัวอย่างด้านหลังแบบฟอร์ม)

☐ **ด้านนโยบาย** **โดยใคร** (กรุณาให้ข้อมูลเจาะจง).....

มีการนำไปใช้อย่างไร

.....

.....

☐ **ด้านสาธารณะ** **โดยใคร** (กรุณาให้ข้อมูลเจาะจง)

.....

มีการนำไปใช้อย่างไร

.....

.....

☐ **ด้านชุมชนและพื้นที่** **โดยใคร** (กรุณาให้ข้อมูลเจาะจง)

.....

มีการนำไปใช้อย่างไร

.....

.....

☐ **ด้านพาณิชย์** **โดยใคร** (กรุณาให้ข้อมูลเจาะจง)

.....

มีการนำไปใช้อย่างไร

.....

.....

√ **ด้านวิชาการ** **โดยใคร** (กรุณาให้ข้อมูลเจาะจง)

จากผลการดำเนินงานโครงการ “จมูกอิเล็กทรอนิกส์แบบไฮบริดที่พัฒนาจากก๊าซเซ็นเซอร์แบบโลหะออกไซด์ร่วมกับก๊าซเซ็นเซอร์แบบนาโนคอมโพสิตเพื่อใช้ในการระบุชนิดของแบคทีเรีย” โดยสามารถพัฒนาระบบหัวตรวจวัดกลิ่นที่เหมาะกับการนำไปใช้ในการจำแนกชนิดของเชื้อแบคทีเรีย ซึ่งโครงการนี้สามารถสร้างองค์ความรู้ใหม่ (Journal paper) นอกจากนี้โครงการนี้ยังนำมาเป็นส่วนหนึ่งในกระบวนการพัฒนาศักยภาพของนักศึกษาในด้านการวิจัย ได้แก่

- นางสาวนภเนตร เรือนเย็น นักศึกษาหลักสูตรปริญญาวิทยาศาสตรบัณฑิต (เทคนิคการแพทย์) คณะเทคนิคการแพทย์ มหาวิทยาลัยมหิดล หัวข้อภาคนิพนธ์ “Development of hybrid gas sensor system for pathogenic bacterial analysis”
- นางสาวภัทรวดี คำม่วง นักศึกษาหลักสูตรปริญญาวิทยาศาสตรบัณฑิต (เทคนิคการแพทย์) คณะเทคนิคการแพทย์ มหาวิทยาลัยมหิดล หัวข้อภาคนิพนธ์ “Development of chemical gas sensor for healthcare and safety applications”

มีการนำไปใช้อย่างไร (กรุณาให้ข้อมูลเจาะจง)

.....

.....

√ **ยังไม่มีการนำไปใช้** (โปรดกรอกในกรอบถัดไป)

(กรณีที่ยังไม่มีการใช้ประโยชน์) ผลงานวิจัยมีศักยภาพในการนำไปใช้ประโยชน์

☐ ด้านนโยบาย ☐ ด้านสาธารณะ ☐ ด้านชุมชนและพื้นที่ ☐ ด้านพาณิชย์ √ ด้านวิชาการ

ข้อเสนอแนะเพื่อให้ผลงานถูกนำไปใช้ประโยชน์

- การตรวจจำแนกชนิดของแบคทีเรียด้วยกลิ่นนี้จำเป็นต้องมีการพัฒนาระบบเพิ่มขึ้นเพื่อให้ง่ายต่อการนำไปใช้จริง และต้องเพิ่มปริมาณตัวอย่างของแบคทีเรียเพื่อหาความแปรปรวนต่างๆเมื่อนำไปใช้จริงในอนาคตต่อไป
- สามารถนำองค์ความรู้ในการพัฒนาก๊าซเซ็นเซอร์ไปปรับเปลี่ยนให้สามารถตรวจวัดก๊าซชนิดอื่นได้ในอนาคต

การเผยแพร่/ประชาสัมพันธ์ (กรุณาให้รายละเอียด พร้อมแนบหลักฐาน)

1. สิ่งพิมพ์ หรือสื่อทั่วไป

☐ หนังสือพิมพ์ ☐ วารสาร ☐ โทรทัศน์ ☐ วิทยุ ☐ เว็บไซต์ ☐ คู่มือ/แผ่นพับ ☐ จัดประชุม/อบรม ☐ อื่น ๆ

.....

.....

2. สิ่งพิมพ์ทางวิชาการ (วารสาร, การประชุม ให้ระบุรายละเอียดแบบการเขียนเอกสารอ้างอิง เพื่อการค้นหาซึ่งควรประกอบด้วย

ชื่อผู้แต่ง ชื่อเรื่อง แหล่งพิมพ์ ปี พ.ศ. (ค.ศ.) ฉบับที่ หน้า)

- **Sumana Kladsomboon**, Chadinee Thippakorn, Thara Seesaard* Development of organic-inorganic hybrid optical gas sensors for the non-invasive monitoring of pathogenic bacteria. Sensors (Switzerland). 2018;18(10).
- Thara Seesaard, Chadinee Thippakorn, Teerakiat Kerdcharoen, **Sumana Kladsomboon*** A hybrid electronic nose system for discrimination of pathogenic bacterial volatile compounds. Analytical Methods. 2020; DOI: 10.1039/D0AY01255F.

Executive Summary

Project Title: Hybrid electronic nose based on metal-oxide semiconductor and nanocomposite gas sensors for bacterial identification

Project Code: MRG6080151

Investigator: Asst. Prof. Dr. Sumana Kladsomboon

Faculty of Medical Technology, Mahidol University

Research problem

Bacterial infection is commonly occurred in the skin and soft tissue for the human. Even though most pathogenic bacteria such as *E. cloacae*, *E. coli*, *P. aeruginosa*, *S. aureus* and *S. Typhi*. can be found in the environment, current technique for bacterial identification, i.e., cell culture method, time at least 24-48 hours and needs specialist to identify. Previous studies found that the pattern of volatile organic compounds (VOCs) which were produced during the bacterial culture period depended on the bacterial species. Moreover, each bacteria species produced specific VOCs profile and generated the unique growth curve. Therefore, the idea to identify bacteria using VOCs profile was studied based on gas sensors and electronic nose (e-nose) technique. In this work, two type of gas sensor e.g. optical gas sensor and nanocomposite gas sensor was developed based on organic-inorganic dyes such as porphyrin and phthalocyanine. Moreover, optical e-nose system and electrical e-nose system were proposed to predict the pathogenic bacterial species based on the volatile organic compound (VOC) from bacteria in culture medium.

Results

For optical e-nose system, the sensitivity and stability of optical gas sensors were enhanced by the thermal treatment process. The in-house optical artificial nose system based on light emitting diode and photo detector was successful to investigate the characteristic of a new optical gas sensor under the dynamic gas flow system. The identification of bacteria was successfully detected by the PCA within the incubation time of 9 hours.

For electrical e-nose system, this system was developed from the hybrid gas sensor platform for nanocomposite gas sensors and metal oxide gas sensors. These gas sensors represented the different pattern of %sensitivity based on the tested volatiles. Moreover, the discrimination of five groups of bacteria was presented by Principal Components Analysis (PCA) at the variation of 99.70% within the 6 hours of incubation period.

sensors

MDPI

Article

Development of Organic-Inorganic Hybrid Optical Gas Sensors for the Non-Invasive Monitoring of Pathogenic Bacteria

Sumana Kladsomboon [1], Chadinee Thippakorn [2] and Thara Seesaard [3,*]

[1] Department of Radiological Technology, Faculty of Medical Technology, Mahidol University, Phutthamonthon, Nakhon Pathom 73170, Thailand; sumana.kla@mahidol.edu
[2] Center for Research and Innovation, Faculty of Medical Technology, Mahidol University, Phutthamonthon, Nakhon Pathom 73170, Thailand; chadinee.thi@mahidol.ac.th
[3] Department of Physics, Faculty of Science and Technology, Kanchanaburi Rajabhat University, Kanchanaburi 71000, Thailand
* Correspondence: thara.seesaard@kru.ac.th; Tel.: +66-86-764-8289

Received: 7 August 2018; Accepted: 18 September 2018; Published: 21 September 2018

Abstract: Hybrid optical gas sensors, based on different organic and inorganic materials, are proposed in this paper, with the aim of using them as optical artificial nose systems. Three types of organic and inorganic dyes, namely zinc-porphyrin, manganese-porphyrin, and zinc-phthalocyanine, were used as gas sensing materials to fabricate a thin-film coating on glass substrates. The performance of the gas sensor was enhanced by a thermal treatment process. The optical absorption spectra and morphological structure of the sensing films were confirmed by UV-Vis spectrophotometer and atomic force microscope, respectively. The optical gas sensors were tested with various volatile compounds, such as acetic acid, acetone, ammonia, ethanol, ethyl acetate, and formaldehyde, which are commonly found to be released during the growth of bacteria. These sensors were used to detect and discriminate between the bacterial odors of three pathogenic species (*Staphylococcus aureus, Escherichia coli and Pseudomonas aeruginosa*) grown in Luria-Bertani medium. Based on a pattern recognition (PARC) technique, we showed that the proposed hybrid optical gas sensors can discriminate among the three pathogenic bacterial odors and that the volatile organic compound (VOC) odor pattern of each bacterium was dependent on the phase of bacterial growth.

Keywords: artificial nose system; metallo-porphyrins; metallo-phthalocyanine; optical gas sensor; bacterial identification

1. Introduction

In the medical care sector, many researchers are striving to exploit the chemistry of bacteria for early detection and surveillance of infectious diseases. Most infections in patients are caused by one of several types of pathogenic bacteria that can be found in the environment: *Staphylococcus aureus*, *Escherichia coli*, *Pseudomonas aeruginosa,* and so on. Many serious infections, such as pneumonia [1], meningitis [2], osteomyelitis [3], toxic shock syndrome [4], bacteremia, and sepsis [5], are often caused by the gram positive bacteria, *S. aureus*. In contrast, two types of gram negative bacteria are prominent for other reasons. *P. aeruginosa* is often the cause of infections in hospitalized patients and has a high rate of resistance to a variety of antibiotics [6]. *E. coli*, which may produce a Shiga toxin, can cause severe illness in humans and food poisoning [7]. Many bacterial species are present in both indoor and outdoor environments and can enter the human body through a break in the skin or mucosa. It is therefore absolutely necessary to determine the presence or absence of pathogenic bacteria prior to starting antibiotics. In general, conventional culture methods used to identify species of bacteria

take at least 12–48 h [8]. Therefore, development of a simple non-invasive method for early detection and identification of bacteria has played a key role in the advancement of medical screening and surveillance. During recent decades there has been increasing interest in developing alternative methods for identification of individual strains of bacteria by the use of specific volatile organic compounds (VOCs) analysis [9]. Several species of bacteria produce unique VOC profiles and may generate characteristic odors [10]. Based on gas chromatography-mass spectrometry (GC-MS) analyses, ammonia is the major VOC from *P. aeruginosa* and *S. aureus* [11,12], while methanol [13], 1-propanol [9], 1-butanol [14], and indole [9] are associated with *E. coli*. Moreover, all bacteria generally produce different amounts of formaldehyde and ethanol vapors during their growing period. Although GC-MS analysis is recognized as a reliable procedure for bacterial identification, there are some problems and limitations that stand in its way, such as high cost and complicated processes. Because of these restrictions, many researchers in the field of sensor technology are trying to develop new techniques for classifying bacteria. Such methods, known as electronic noses, will make operations faster and easier than ever before [15]. Artificial nose systems are used to convert chemical information regarding volatile molecules into electrical signals. These consist of three components, each with a specific duty: (i) chemical vapor detection with gas sensor array platforms; (ii) signal processing; and (iii) pattern recognition [16–18]. Pattern recognition methods and algorithms are commonly employed in reusable, sensor-based VOC detection with real samples that can be directly analyzed without complicated sample preparation [19]. Therefore, these methods will not only be helpful in sensor array research for detection of odor signatures for screening and early identification, but also have great potential for clinical application without special laboratory equipment [20].

The optical gas sensor is one of many categories of gas sensor technology that can be investigated scientifically based on a common analytical instrument such as the UV-Vis spectrophotometer [21]. For example, an optical gas sensor combined with an electronic nose system is capable of monitoring for food spoilage based on the VOCs production from specific bacterial activity [22]. Selection of optical materials for sensor design and fabrication depends on a variety of factors such as the strength of reaction between the sensing material and one or more of the target odor compounds. Other factors are the color change which occurs during the gas absorption and the stability of sensors [23]. In general, optical gas sensors are usually fabricated from two types of organic dyes, metallo-porphyrins and metallo-phthalocyanine, which are both antibacterial compounds [24,25]. These organic dyes have markedly extended π-electron systems and exhibit stability at room temperature [26]. Modifications of the basic skeletons and central metal atom of the sensing materials lead to their remarkably high sensitivity to VOCs [27]. The sensitive area of the sensor is frequently observed in the near Q and B band regions of the light absorption spectrum [28]. Based on quantum mechanical (QM) calculations, there is a transfer of electric charge between the analyte gas and the central metal atom of the organic dye that indicates a potential change of their optical spectrum [29]. The metallo-porphyrins and metallo-phthalocyanine mentioned above were discovered to be excellent sensing materials for optical gas sensors based on changes in optical absorption of amorphous thin films. Specifically, zinc-porphyrin [30], manganese-porphyrin [31], and zinc-phthalocyanine [31,32] are used as common gas sensors for detection of various types of VOCs such as alcohol, acid, ketone, amine, and aldehyde. In terms of gas sensing properties, surface structure modification of sensing materials has the potential to enhance the sensing properties of gas sensors. Surface morphology of the films has changed greatly due to the thermal treatment process [33]. This process affects optical properties, such as absorption spectrum, that are related to the sensitivity of the sensors. For example, optimization of the grain size of thin-surface-layers can be expanded to provide greater surface area of the gas sensor for interaction with the absorbed analyte molecules [34]. Such research has yielded many useful fabrication processes for development of better optical gas sensors. However, there is no published work related to the fabrication of organic-inorganic hybrid, optical gas sensors with three different types of dye (zinc-porphyrin, manganese-porphyrin, and zinc-phthalocyanine). Therefore, our research work extended the functionality of optical gas sensors that generate a wide range of

absorption spectra. Moreover, the optical gas sensors we fabricated have many advantages such as increasing the active sites for gas detection to improve the gas sensor response. Thus, the emergence of a hybrid optical gas sensor based on three types of dye will open new frontiers in pathogenic bacteria odor monitoring.

Accordingly, the aim of this study was to assess the feasibility and performance of optical gas sensors based on an artificial nose system for the rapid detection and classification of bacterial pathogens, specifically *P. aeruginosa*, *E. coli* and *S. aureus*. The optical gas sensors were fabricated from three organic-inorganic hybrid materials. Sensitivity of these sensors was enhanced by thermal treatment. Statistical methods, such principal components analysis (PCA), were used to identify the pattern recognition and classification of VOCs from the three different bacterial species grown in culture medium. In addition, we evaluated the accuracy in each change of signal-response using the *p*-value method (Hypothesis testing). Results of this study may provide data to consider in choosing specific optical gas sensors that are appropriate for detection of bacterial odors in order to protect the public from bacterial contamination of food and drink in the manufacturing industry and in the environment.

2. Materials and Methods

2.1. Optical Gas Sensor Fabrication

Zinc-5,10,15,20-tetra-phenyl-21H,23H-porphyrin (ZnTPP), zinc-2,9,16,23-tetra-tert-butyl-29H, 31H-phthalocyanine (ZnTTBPc), and manganese (III)-5,10,15,20-tetraphenyl-21H,23H-porphyrin chloride (MnTPPCl) were purchased from Sigma-Aldrich (St. Louis, MO, USA). The ZnTPP, ZnTTBPc, and MnTPPCl were dissolved in chloroform at the concentrations 5, 10 and 15 mg/mL, respectively. Then, equal volumes of the three solutions were mixed together. Then, 0.5 mL of the mixed solution was deposited on clean glass substrates, using the spin coating method at a speed of 1000 rpm for 30 s. Finally, the sensing films were enhanced by thermal treatment for 30 min at 150 °C under air atmosphere.

2.2. Characterization of the Hybrid Optical Gas Sensor

Change of optical absorption spectra of gas sensors for both the non-treated and treated sensing films were investigated with a UV-Vis spectrophotometer (Shimadzu UV-2450, Tokyo, Japan). The hybrid optical gas sensors were placed into a stable VOC atmosphere chamber to observe their sensitivity to six vapors: acetic acid, acetone, ammonia, ethanol, ethyl acetate, and formaldehyde. The absorption index of gas sensors when tested along with each VOC were recorded in the visible spectral range of 300–700 nm. Moreover, the optical gas sensors' sensitivity under dynamic gas flow conditions was investigated by an optical artificial nose system (see Figure 1). All tested VOC solutions were prepared at the concentration of 10% (volume/volume) in water. Once a VOC sample was incorporated into a sample bottle, the operating temperature was adjusted for each VOC sample to control for the same evaporating pressure of each VOC through the sensor chamber. In addition, a nitrogen carrier system was installed inside the system to spread the VOC's vapor evenly across the bottle, delivering volatile vapors to the sensor chamber. Two cases of the non-treated and treated gas sensors were consecutively exposed to the VOCs for 2 min and N_2 for 2 min at room temperature. Lastly, structure and morphology of the gas sensor were measured by atomic force microscopy (Agilent 5500 AFM, Agilent Technologies, Chandler, AZ, USA).

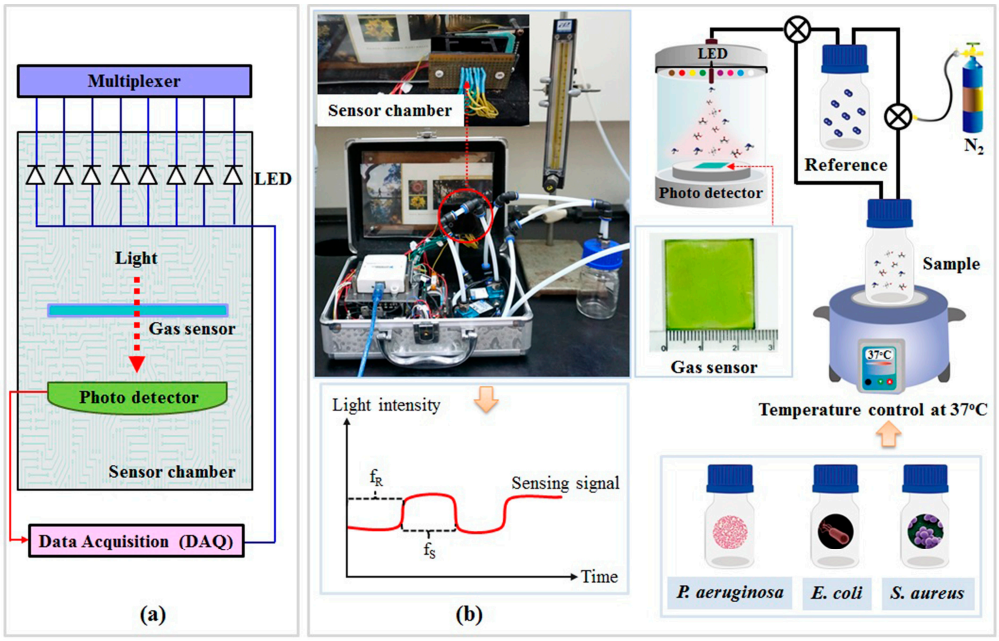

Figure 1. Schematic diagram of the optical artificial nose system, including (**a**) measurement/controller circuit section and (**b**) odor delivery section.

2.3. Optical Artificial Nose System

The optical artificial nose system for odor detection was composed of a hybrid optical sensor and data acquisition algorithm. The schematic diagram of the in-house artificial nose system is shown in Figure 1. This system involves two main elements: measurement/controller circuit section and odor delivery section. A National Instruments data acquisition (Ni-DAQ) USB-6008 card with LabVIEW was chosen as the measurement and the control device (analog input and digital output), see Figure 1a. Low cost commercial LED lamps were used to create an artificial light source. Each channel of the analog multiplexer selected one of several input signals from individual LED lamps and forwarded the selected input into a single line to the output signal frequency of each LED lamp. The optical transducer (CMOS photo-detector), which converted light into an electrical quantity, was chosen to collect the light intensity transmitted through the optical gas sensor. This photo-detector was the color light-to-frequency converter module (TCS230) from Texas Advanced Optoelectronic Solutions Company (Plano, TX, USA). The output data was constructed as a square wave with frequency directly proportional to light intensity. Wavelengths corresponding to red, yellow, green, pink, blue, and violet LEDs were centered at 638, 587, 537, 472, 457, and 399 nm, respectively, while white and infrared LEDs represented the broad spectrum light around 450–700 and 700–1 $\times$ 10^6 nm, respectively. The intensity of light transmitted through the optical gas sensor was detected from the photon frequency (Hz) that interacted directly with the photo-detector during the dynamic gas flow measurement, see Figure 1b. An array of optical gas sensors was generated with LED lights of eight colors (infrared, red, yellow, green, violet, pink, blue, and white). Nitrogen gas (N_2) was used as the pure carrier (reference) gas, delivering odors to the sensor chamber. The flow rate of the N_2 gas was controlled by a mass flow meter at a constant rate of 700 mL/min. Measurement of the dynamic gas flow system was performed by switching between the sample gases for 2 min and the N_2 for 2 min. This process was repeated for 5 cycles. The gas sensing response (S) from the eight sensors was the difference between the maximum peak (signal frequency from the sample odor) and the baseline (signal frequency from the reference gas). These responses were used as the input data for pattern recognition by principal component

analysis (PCA). The gas sensing response (S) was defined as the light intensity change in the frequency during the presence of dynamic gas flow measurements as follows (Equation (1)):

$$S = \left(\frac{f_S - f_R}{f_R}\right) \times 100 = \left(\frac{\Delta f}{f_R}\right) \times 100 \quad (1)$$

where f_R is the initial frequency of each optical wavelength without the sample vapor (baseline frequency) and f_S is the frequency when exposed to the testing gas vapor, see in Figure 1b. The gas sensing response (S) can be calculated from a differential comparison between the initial frequency of each optical wavelength (baseline frequency or f_R) and the frequency when exposed to the testing gas vapor (f_S). Therefore, spectral sensitivity can be represented as a percentage of the changes in the frequency signal relative to the initial frequency of each optical wavelength.

2.4. Bacterial Cultures

Three standard strains of bacteria were selected for this study. *Staphylococcus aureus subsp. aureus* (ATCC 29213), *Escherichia coli* (ATCC 25244), and *Pseudomonas aeruginosa* (ATCC 27853) were obtained from the Faculty of Medical Technology, Mahidol University, Thailand. They were cultured in sterile nutrient medium and incubated at the optimum temperature for growth. Briefly, batch cultivation was carried out in Luria-Bertani (LB) medium at 37 °C. The composition of the LB broth per liter was Tryptone (Difco Laboratories) 10 g, Yeast extract (Difco) 5 g, and NaCl 5 g. Medium was made using distilled water and adjusted to within a pH range of 7.2–7.4 using diluted solutions of NaOH and then autoclaved under standard conditions of temperature and pressure (121 °C at 15 psi) for 15 min (followed the Miller's formula). Single bacterial colonies from LB agar plates were inoculated into 5 mL of LB broth and maintained at 37 °C for 9 h in a shaking incubator (180 rpm). After incubation, bacterial growth was characterized by a cloudy media. The concentration of bacteria in medium was obtained by a measurement of the optical density at 600 nm (OD600) of the culture suspensions with a UV-Visible spectrophotometer. The three different types of initiating bacterial cultures were adjusted until the OD600 was equal to 0.3. Then, each bacterial culture was inoculated into 25 mL of LB broth to control the initial bacterial counts in the sample bottles for odor detection.

Bacterial cultures were maintained at a constant incubation temperature (IT) of 37 °C. Culture samples were removed at intervals and the numbers of viable bacteria were counted (the increasing turbidity assessed at OD600). A logarithmic growth curve of each bacterial strain was plotted. Finally, the OD600 value and gas sensing response of each bacterial culture were collected and recorded every 3 h.

3. Results and Discussion

3.1. Optical Gas Sensor Characterization

In this work, the hybrid optical gas sensor was fabricated by employing metal-free organic-inorganic dyes, namely ZnTPP, ZnTTBPc, and MnTPPCl. Effects of thermal treatment on the structure and the sensitivity properties of the optical gas sensor were investigated by UV-Vis spectroscopy. Figure 2 shows the changes in the absorption spectrum of optical gas sensors with and without thermal treatment. Six volatile compounds (10% in water, acetic acid, acetone, ammonia, ethanol, ethyl acetate and formaldehyde) associated with bacterial metabolism and released during bacterial growth were selected for the testing of sensor performance [10–14]. In the case of the non-treated gas sensor, maximum absorptions centered at 345, 430, 480, 564, 615, and 690 nm (see Figure 2a). The Soret bands of ZnTTBPc, ZnTPP, and MnTPPCl are the absorption peaks at 345, 430, and 480 nm [30], respectively. The absorption bands observed in the 400–500 nm range are related to n-π^* transitions of the lone nitrogen pair orbital of the macrocycle. The peaks at 564 and 615 nm are the Q bands of porphyrin compounds, while the peak at 690 nm is the Q band of the ZnTTBPc. These Q bands are related to the π-π^* transitions of the porphyrin macrocycle ring [35]. The shift of

the absorption spectra in both cases (with and without thermal treatment) of the gas sensors when exposed to VOs vapors were observed near the main peaks, namely 345, 430, 480, and 690 nm (see Figure 2a,b). These absorption spectral shifts of the gas sensors are related to the electron interchange between the analyte gas and π-π conjugated system of the porphyrin molecule that effects the electron density π-π* transitions [36]. Our results showed that the absorption spectra of the thermal-treated gas sensor had much stronger changes than did the non-treated sensor, especially at 345, 430, and 480 nm. Therefore, the absorption spectral changes of the Q and B bands of the gas sensor were calculated with special attention.

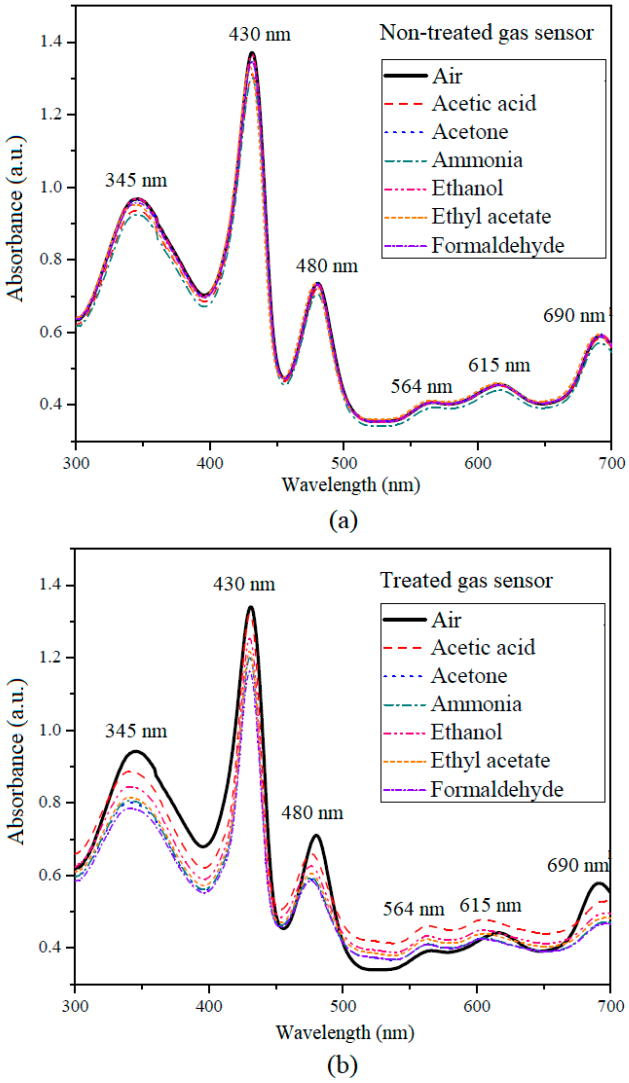

Figure 2. UV-Visible absorption spectra changes of (**a**) non-treated and (**b**) thermally treated gas sensors with volatile organic compound (VOC) exposure.

The changes in the absorption spectra of the optical gas sensors between the atmospheric N_2 and the six volatile organic compounds representative of those released during bacterial growth were calculated using Equation (2) below.

$$A_W^S - A_W^R \quad (2)$$

where A_W^S is the absorption spectrum of the analyte gas at w wavelength and A_W^R is the absorption spectrum of the reference gas at w wavelength.

Figure 3a shows the change in the absorption spectra of the non-treated gas sensor with six VOCs at 345, 430, 480, and 690 nm. Almost all absorption spectrums of the gas sensor were decreased after exposure to the VOC vapors. The highest absorbance value was observed at 430 nm, which is the B band of porphyrin. The sensitivity of the optical gas sensor can be calculated from the changes in the absorption spectrum values of thermal treatment compared with those of the non-thermal treatment (see in Figure 3a,b). It can be seen that the changes in the absorption spectrum of the thermally treated gas sensor were higher than that of the non-treated gas sensor for all wavelengths.

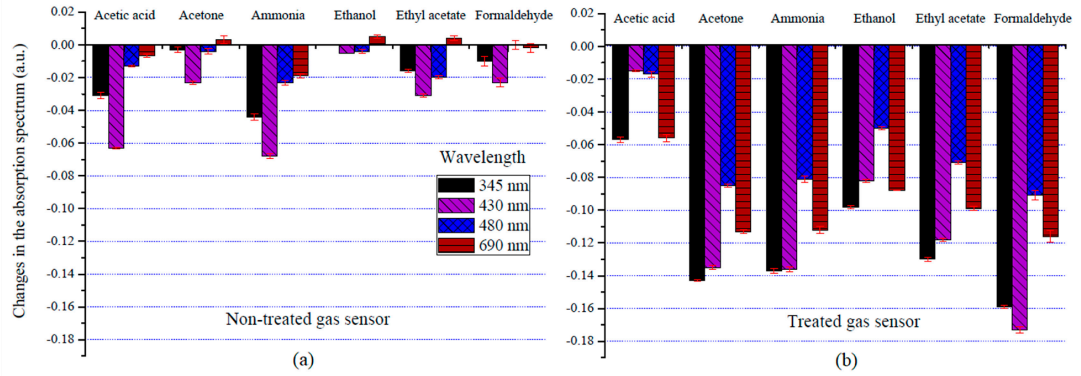

Figure 3. Changes in the absorption spectrum of (**a**) non-treated and (**b**) thermally treated gas sensors with different VOC profiles at wavelengths of 345, 430 480, and 690 nm.

Wavelengths of 345 and 430 nm were associated with higher responses than at other wavelengths, particularly in the response patterns of the six VOCs measured by UV-Visible spectroscopy. Moreover, the changes in the absorption spectra of the treated gas sensor with the VOCs tested were found to peak at approximately 430 nm, especially with formaldehyde vapor. In addition, the electric charge transferred between the analyte gas and the central metal atom of the organic dye during the interaction process can be explained by the quantum mechanical (QM) calculations based on density functional theory (DFT). The electric charge of dye molecule was significantly changed after chemisorption of the gas molecule at the central metal atom [30]. Subsequently, this charge transport path depends on the position of dye molecule on the substrate [29]. Thus, this calculation indicates that electric charge transfer has the potential to change the optical spectrum of organic dye.

The surface morphology of non-treated and treated gas sensors were characterized by using atomic force microscopy (AFM) as shown in Figure 4. The surface roughness of thin-film gas sensors for non-thermal treated and thermal treated film were 0.494 and 0.961 nm, respectively. Thus, the thermal treatment process can promote changes from a smooth surface to a knobbed surface [33]. Moreover, the average hole size of a thermal treated gas sensor was 0.1 μm, while the hole sizes of a non-treated gas sensor cannot be evaluated due to the smooth surface. It was evident that the surface morphology changed upon thermal treatment, and that surface roughness increased. This type of modified surface is associated with optimized trace gas detection due to shifts in the absorption spectra of the gas sensors [34], as can be seen in the bar graph (Figure 3) and the AFM images (Figure 4). Moreover, the AFM results in Figure 4 indicate that the thermal treatment has an effect on the structure and surface area on gas sensing films, leading to an increase of surface roughness. According to existing research, the temperature used in thin film preparation affects the morphology of the film's surface [33]. Therefore, increasing the surface area of films generally enhances the rate of a chemical vapor reaction [34], which leads to the significant increase in the sensor's response, as shown in Figure 3.

Figure 5 shows a comparison of the gas sensing response (S) of the thermally treated gas sensor when exposed to different VOCs (10% in water) under dynamic gas flow conditions. An in-house optical-based artificial nose system was developed to study the performance of thin-film sensing materials. The gas sensing response (S) was calculated from the light intensity change between the

sensor signal without sample vapor (baseline light intensity, f_R) and the signal when exposed to the test vapor (f_S) (see Equation (1)).

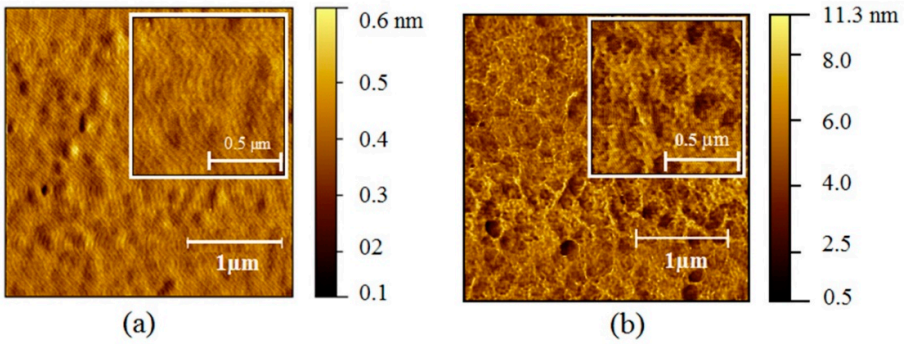

Figure 4. Atomic force microscopy (AFM) images (1 μm) of (**a**) non-treated and (**b**) thermally treated gas sensors.

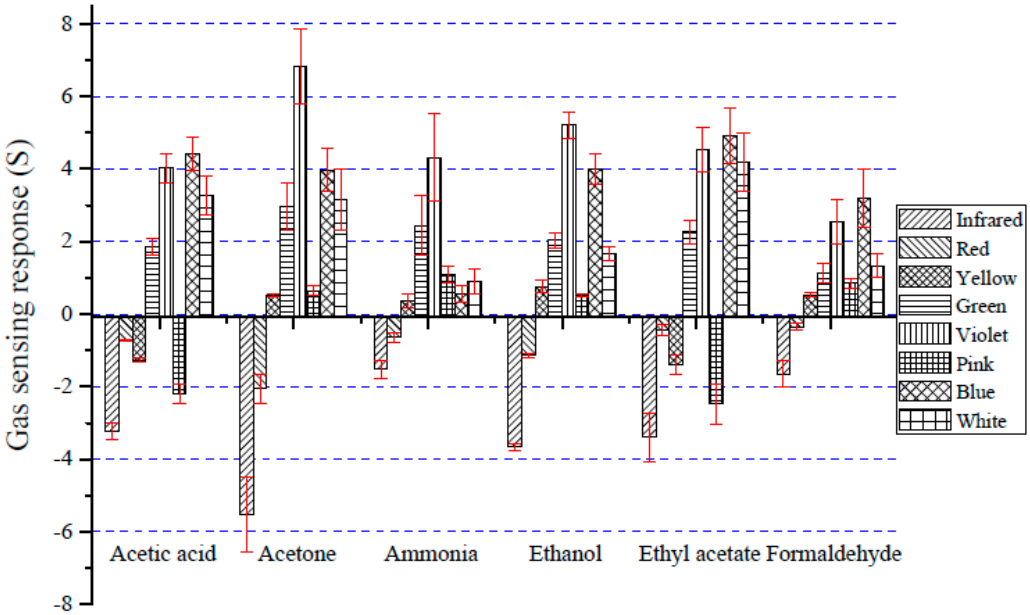

Figure 5. The gas sensing response (S) of thermally treated gas sensors toward VOCs in water (10%, volume/volume) under dynamic gas flow conditions.

An array of eight optical gas sensors was generated from the different LED light sources: infrared, red, yellow, green, violet, pink, blue, and white. The sensitivity of gas sensors depends on the LED light source and the types of VOCs. The sensing signals from the yellow, green, violet, blue, and white LEDs showed positive S values, while the infrared, red, yellow, and pink LEDs showed negative S values. These results showed that light intensity changed when the sensors were placed in the vapor flow of the sampling system. Excellent sensing behavior was found in the case of the violet, blue, infrared, and white LEDs for all VOCs, demonstrating that the most active sites for sensing signals were at 399 nm, 457 nm, the infrared region, and broad spectrum light. The highest sensing response to the gases was found with acetone vapor and the violet LED. The gas sensor had distinct response patterns with different gases, which represented the odors that are released during bacterial growth. Therefore, the thermally treated gas sensor is proposed for bacterial identification.

3.2. Bacterial Growth and Pattern Analysis

Bacterial populations were quantitated periodically, and the number of viable bacteria was plotted on a log graph against time. This gives a bacterial growth characteristic which is known as the growth

curve or growth cycle. Here, the growth of each bacterial strain in liquid media was investigated by observing the OD600 as shown in Figure 6. The absorption of this media was investigated (in triplicate) at the wavelength of 600 nm. An exponential growth phase was observed during the 24-h incubation. There were different growth characteristics for the three pathogens, and each had a high R-squared (R^2) value. The growth rate of *P. aeruginosa* was compared with those of *S. aureus* and *E. coli* (R^2 values of 0.9881, 0.9619, and 0.9214, respectively). The results indicated that the growth rate of E. coli was a bit less than those of *P. aeruginosa* and *S. aureus*. Moreover, the stationary phase (no further increase in the number of cells) of all three bacterial strains was observed after 16 h of incubation. The hybrid optical gas sensor was applied to investigate the relationship between the bacterial activity and VOC release.

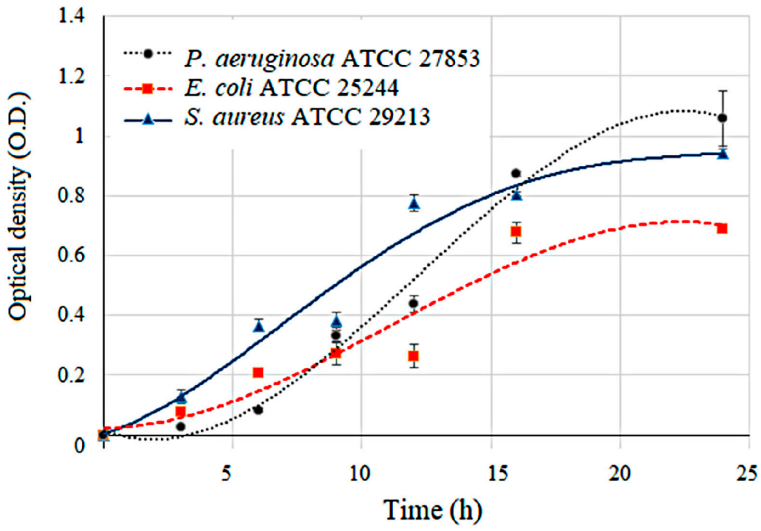

Figure 6. The optical density at 600 nm (OD600) was plotted versus time for individual pathogens in culture over an incubation period of 24 h. The growth curves were distinct for each pathogen. Blue triangle, red square, and black circle represent the data points used to construct the growth curves of *S .aureus*, *E. coli*, and *P. aeruginosa*, with R-squared (R^2) statistics of 0.9628, 0.9214 and 0.9881, respectively.

The hybrid optical gas sensor was used to detect the volatiles produced by the three pathogenic bacteria and the pathogen-free LB media. Figure 7 illustrates the results of the optical gas sensor array signal from bacteria growing over a 9-h incubation. Nitrogen gas was used for gas-flushing to clean the chamber and also used as a carrier gas to deliver the odor to the sensor chamber. While conducting the measurement, all culture samples were maintained at a controlled temperature of about 37 °C. The sensorgram showed the level of the light intensity signal obtained from the optical sensor array. The design consisted of an eight-channel gas sensor, generated from eight LED light sources, namely infrared, red, yellow, green, blue, pink, violet, and white LED.

The measurement was performed by switching between the nitrogen gas for 2 min and the sample vapor for 2 min. This process was repeated five times for one measurement. The optical sensing signal was investigated in the form of photon frequency (kHz) and recorded every 4 s. Increased optical sensing signals were found with the green, blue, violet, and white LEDs, while decreased optical sensor signals were found with the infrared, red, yellow, and pink LEDs. The optical sensing signals of *P. aeruginosa* and *S. aureus* were found prominently displayed with all LED light sources, but *E .coli* was not observed with the red and yellow LEDs. Therefore, the optical sensing signal patterns of *P .aeruginosa* and *S. aureus* were different from those of *E. coli.* Even though the optical sensing signal patterns of *P. aeruginosa* were similar to those of *S. Aureus*, the optical sensing signal paths differed. Thus, optical gas sensors have a great potential to detect and classify these three pathogenic bacteria based on sensing signal pattern analysis.

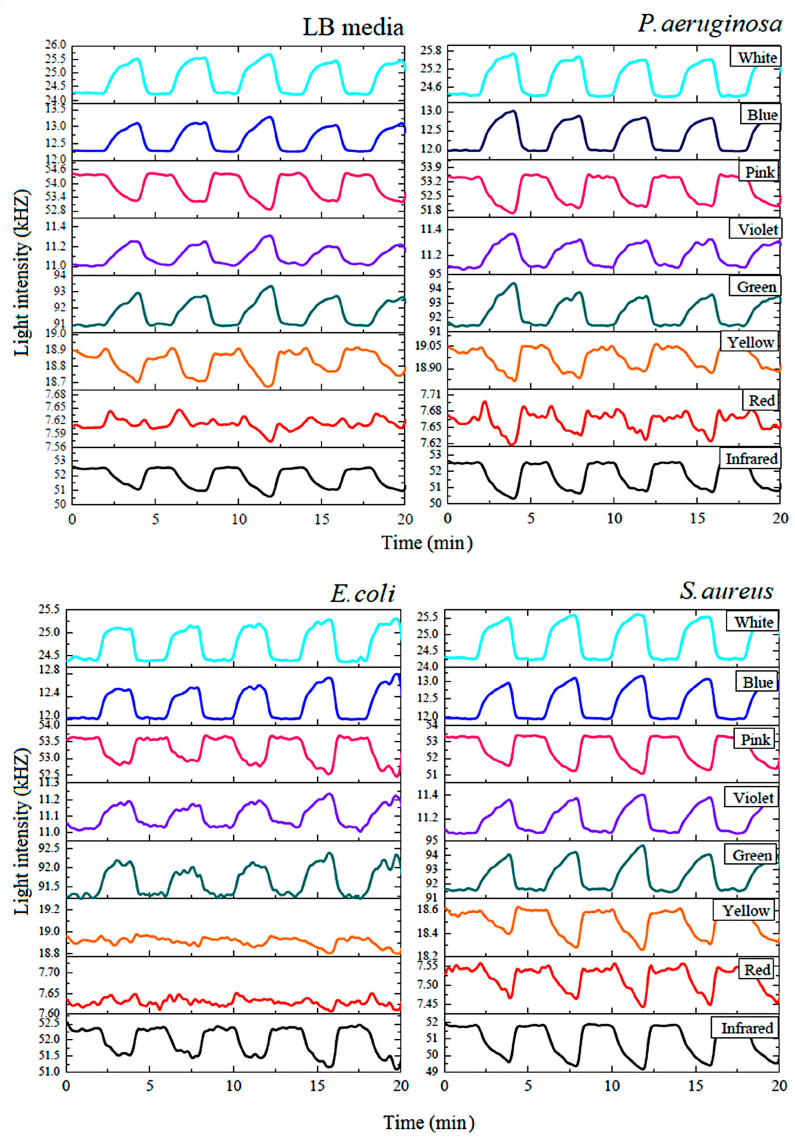

Figure 7. The gas sensing signal of the thermally treated gas sensor with Luria-Bertani (LB) media and the three types of bacteria as measured by the in-house, optical artificial nose.

To evaluate the optical gas sensor's potential for bacterial identification, we exposed it to the VOCs of three bacteria: *P. aeruginosa*, *S. aureus* and *E. coli*. The average percent change in the light intensity of optical sensors under the dynamic measurement system when exposed to volatile gas samples were calculated according to Equation (1). The results (Figure 8) indicated not only that blue LED showed the highest sensing response for the three types of bacteria, but also showed that the bacteria produce a wide range of VOCs in the differing patterns of exponential growth, under standard nutritional conditions (see Figure 6). These sensing responses of optical gas sensors are related to the amount and type of VOCs that are emitted during bacterial activity [37].

Additionally, hypothesis testing (p-value approach) was used to compare the sensor's response to each of the three bacterial species and the LB media control at four different incubation times: 3, 6, 9, and 12 h. Their statistical significances (p-value in brackets) were all highly significant: infrared (0.00001), red (0.00000), yellow (0.00003), green (0.00008), violet (0.00058), pink (0.00000), blue (0.00004), and white (0.00021). This indicated that all optical gas sensors (with incubation time of 9 h) showed a significant difference in the sensor's response between the three types of bacteria and LB media. However, the responses from the red sensor (0.36455) with an incubation time of 3 h were not significantly different among the bacteria samples and the LB media control.

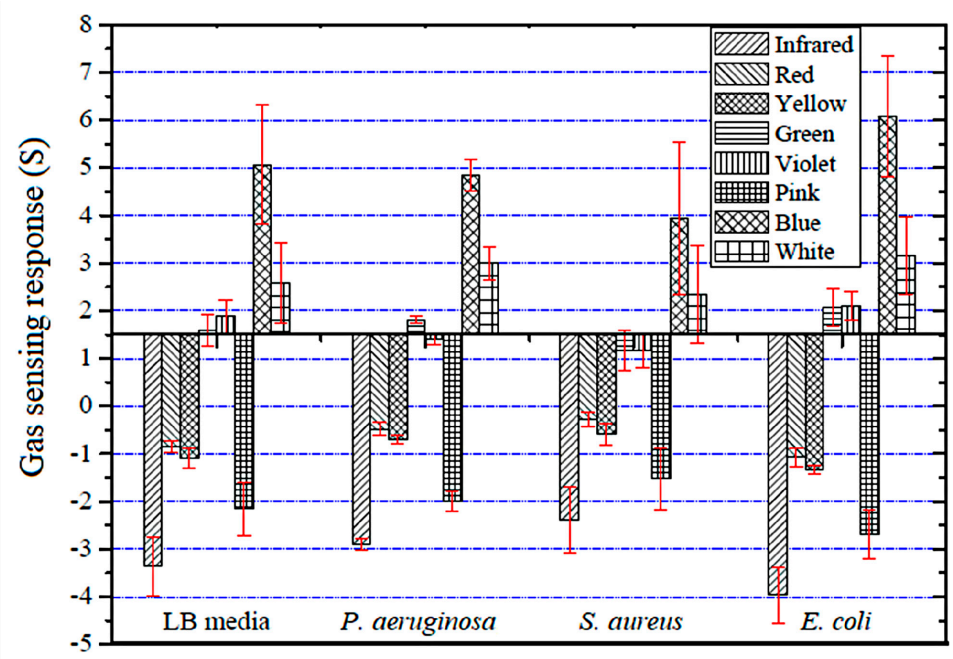

Figure 8. The gas sensing response (S) of the thermally treated optical gas sensor toward three species of bacteria in culture media after 9 h of incubation.

An artificial nose technique was used to identify the physical features of odor patterns from the responses of all the sensors and to distinguish this pattern from a diverse range of smells (odor fingerprint of VOCs released by bacteria). Responses of optical gas sensors to odorants are generally considered as a first order time response. The first step in odor analysis is to flush a reference gas (N_2) through the optical sensor to obtain a baseline. Then, the optical gas sensor is exposed to gas coming from the growing bacteria. This causes changes in the sensor's output signal until a steady state is reached. Three major physical features were captured mathematically as min-max values, slope values, and integral area values and were selected for a feature extraction technique based on analysis of the covariance between the factors. Principal component analysis (PCA) is suitable for multi-dimensional datasets as in this work where data are collected from eight optical sensor arrays and multiple odors. The complex data set (with multiple dimensions) can be transformed using a matrix that represents general values in the form of a new data set (2 or 3 dimensions) [18]. In general, the PCA process consists of several steps which include: (i) preparing the raw data into a data matrix; (ii) scaling a data matrix by normalizing; (iii) calculating a covariance matrix; and (iv) rearranging the eigenvectors and eigenvalues. Then, the PCA result is obtained by matrix multiplication and transposition. The PCA results in this work were presented in the form of new principal components (PCs). The first principal component (PC1) contained more of the data variance of a data set than subsequent components (i.e., PC2 and PC3) [37].

Figure 9 shows the identification of three types of pathogenic bacteria and LB media in PCA plots. To see the effect of incubation period on growth and bacteria activity, a change in smell was investigated every 3 h. It was found that the pure LB medium, *P. aeruginosa*, *S. aureus*, and *E. coli* could be distinguished and grouped using the eclipses with 95% confidence. Figure 9a–d show the distinct clusters of pure LB media and the three bacteria samples, which are separated into four groups even at the earliest assessment (Figure 9a). After 9 h of incubation, discrimination between the different types of bacteria and LB media sample was seen (Figure 9c). PC1 accounts for the greatest variance (95.10%). Thus, it was found that the four data clusters are clearly separated on the PC2 axis, while the data points of the bacteria odors and LB media are scattered along the PC1 axis.

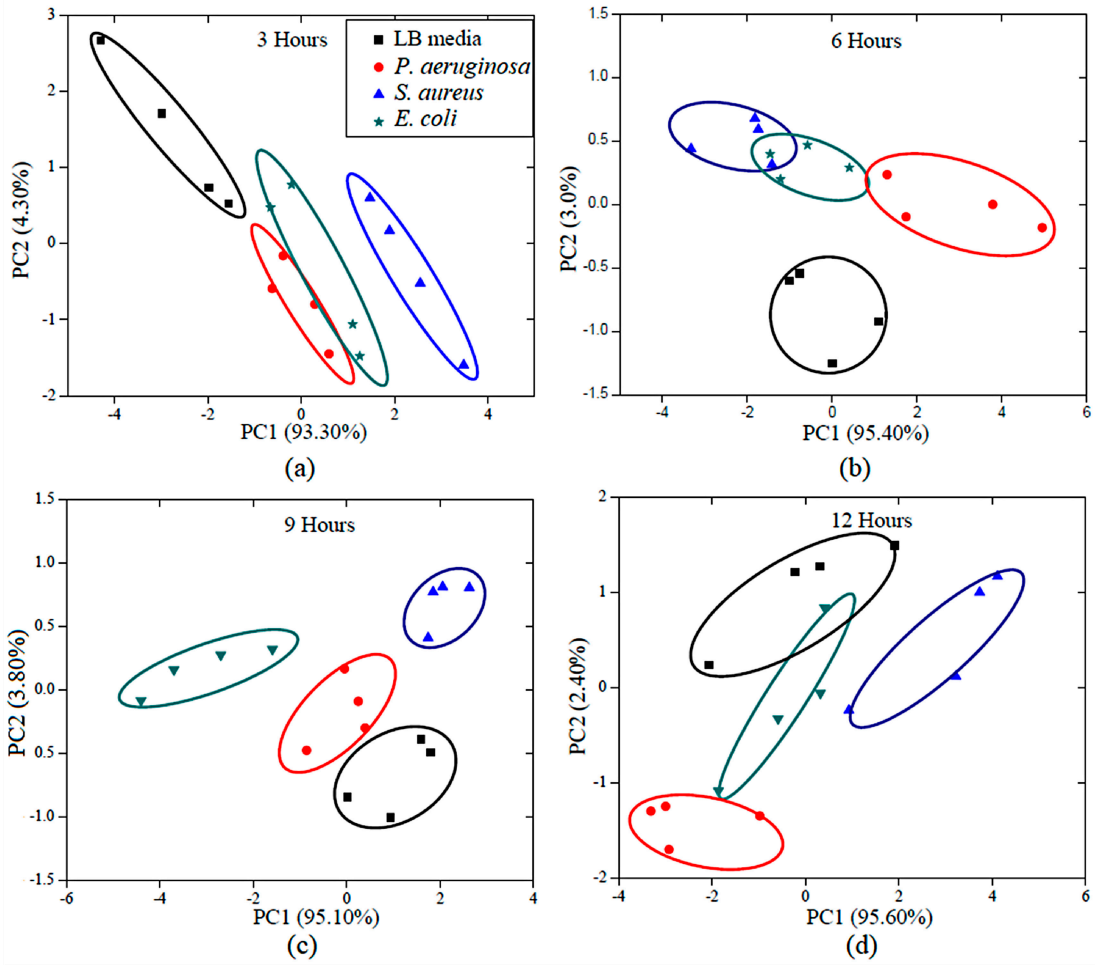

Figure 9. Schematic diagram of principal component analysis (PCA) of three types of pathogenic bacteria in medium with in-house artificial nose measurements at (**a**) 3 h, (**b**) 6 h, (**c**) 9 h and (**d**) 12 h.

PCA results, with several incubation times, odor from three bacteria (*P. aeruginosa*, *E. coli*, and *S. aureus*), and the medium control, appeared close together on the PCA. This result agreed with the gas sensing response results from the VOCs emitted by the selected bacteria at different incubation times (see Figure 8). As a matter of fact, VOCs emitted by the different bacteria varied with stage of growth, which may be due to physical specificity, metabolic influences, or even time-dependent sampling [38]. It was found that the incubation time of 9 h gave each of three types of bacteria a unique pattern of odor (smell fingerprint), as their odor differed not only from each other, but also from the scent of the culture medium. These findings will pave the way for further development of specifically designed, optical gas sensors and artificial nose systems for bacterial odor detection which are both sensitive and specific.

4. Conclusions

The sensitivity and stability of hybrid optical gas sensors were enhanced by a thermal treatment process. The in-house optical artificial nose system based on a light emitting diode and photo detector was successful in investigating the characteristics of a new optical gas sensor within a dynamic gas flow system. The bacteria were successfully detected and identified by the PCA using an incubation time of 9 h. The results showed the feasibility of using an optical artificial nose system for real-time discrimination of bacteria odors to indicate the presence of different bacterial species and their phase of growth. The capability to detect various VOCs as related to the bacteria growth, especially acetic acid, acetone, ammonia, ethanol, ethyl acetate, and formaldehyde, has been demonstrated. Based on pattern

recognition techniques for odor discrimination in optical gas sensor arrays, we have shown that the proposed hybrid optical sensing material combined with an artificial nose system can discriminate the odor of three bacteria species and allow non-invasive pathogenic bacterial monitoring.

Author Contributions: S.K. conceived and designed the experiments, manufactured the sensors, and performed various measurements. She also developed the first draft of the manuscript. C.T. supported S.K. for bacterial sample preparation. T.S. set the focus and the direction of this research, analyzed the sensor response, and also supported the preparation of the manuscript and its editing.

Funding: This project was supported by Mahidol University and the Thailand Research Fund (TRF) (Grant No. MRG6080151).

Acknowledgments: The authors would like to express thanks to Teerakiat Kerdcharoen, Department of Physics, Faculty of Science, Mahidol University, for his assistance and suggestions regarding the artificial nose technique.

Conflicts of Interest: The authors declare that they have no conflicts of interest.

References

1. Abeyrathne, C.D.; Huynh, D.H.; McIntire, T.W.; Nguyen, T.C.; Nasr, B.; Zantomio, D.; Chana, G.; Abbott, I.; Choong, P.; Catton, M.; et al. Lab on a chip sensor for rapid detection and antibiotic resistance determination of Staphylococcus aureus. *Analyst* **2016**, *141*, 1922–1929. [CrossRef] [PubMed]
2. Mellata, M.; Johnson, J.R.; Curtiss, R. Escherichia coli isolates from commercial chicken meat and eggs cause sepsis, meningitis and urinary tract infection in rodent models of human infections. *Zoonoses Public Health* **2018**, *65*, 103–113. [CrossRef] [PubMed]
3. Park, K.H.; Cho, O.H.; Jung, M.; Suk, K.S.; Lee, J.H.; Park, J.S.; Ryu, K.N.; Kim, S.H.; Lee, S.O.; Choi, S.H.; et al. Clinical characteristics and outcomes of hematogenous vertebral osteomyelitis caused by gram-negative bacteria. *J. Infect.* **2014**, *69*, 42–50. [CrossRef] [PubMed]
4. McCormick, J.K.; Yarwood, J.M.; Schlievert, P.M. Toxic shock syndrome and bacterial superantigens: An update. *Annu. Rev. Microbiol.* **2001**, *55*, 77–104. [CrossRef] [PubMed]
5. Herwald, H.; Mörgelin, M.; Björck, L. Contact activation by pathogenic bacteria: A virulence mechanism contributing to the pathophysiology of sepsis. *Scand. J. Infect. Dis.* **2003**, *35*, 604–607. [CrossRef] [PubMed]
6. Chen, Y.; Cheng, N.; Xu, Y.; Huang, K.; Luo, Y.; Xu, W. Point-of-care and visual detection of P. aeruginosa and its toxin genes by multiple LAMP and lateral flow nucleic acid biosensor. *Biosens. Bioelectron.* **2016**, *81*, 317–323. [CrossRef] [PubMed]
7. Rijal, K.; Mutharasan, R. A method for DNA-based detection of *E. coli* O157: H7 in a proteinous background using piezoelectric-excited cantilever sensors. *Analyst* **2013**, *138*, 2943–2950. [CrossRef] [PubMed]
8. Inglis, T.J.J.; Hahne, D.R.; Merritt, A.J.; Clarke, M.W. Volatile-sulfur-compound profile distinguishes *Burkholderia pseudomallei* from *Burkholderia thailandensis*. *J. Clin. Microbiol.* **2015**, *53*, 1009–1011. [CrossRef] [PubMed]
9. Boots, A.W.; Smolinska, A.; Van Berkel, J.J.B.N.; Fijten, R.R.R.; Stobberingh, E.E.; Boumans, M.L.L.; Moonen, E.J.; Wouters, E.F.M.; Dallinga, J.W.; Van Schooten, F.J. Identification of microorganisms based on headspace analysis of volatile organic compounds by gas chromatography-mass spectrometry. *J. Breath Res.* **2014**, *8*. [CrossRef] [PubMed]
10. Wiesner, K.; Jaremek, M.; Pohle, R.; Von Sicard, O.; Stuetz, E. In Monitoring of bacterial growth and rapid evaluation of antibiotic susceptibility by headspace gas analysis. *Procedia Eng.* **2014**, 332–335. [CrossRef]
11. Zscheppank, C.; Wiegand, H.L.; Lenzen, C.; Wingender, J.; Telgheder, U. Investigation of volatile metabolites during growth of Escherichia coli and Pseudomonas aeruginosa by needle trap-GC-MS. *Anal. Bioanal. Chem.* **2014**, *406*, 6617–6628. [CrossRef] [PubMed]
12. Thorn, R.M.S.; Reynolds, D.M.; Greenman, J. Multivariate analysis of bacterial volatile compound profiles for discrimination between selected species and strains in vitro. *J. Microbiol. Meth.* **2011**, *84*, 258–264. [CrossRef] [PubMed]
13. Bos, L.D.J.; Sterk, P.J.; Schultz, M.J. Volatile metabolites of pathogens: A systematic review. *PLoS Pathog.* **2013**, *9*. [CrossRef] [PubMed]
14. Tait, E.; Perry, J.D.; Stanforth, S.P.; Dean, J.R. Identification of volatile organic compounds produced by bacteria using HS-SPME-GC-MS. *J. Chromatogr. Sci.* **2014**, *52*, 363–373. [CrossRef] [PubMed]

15. Peng, C.; Yan, J.; Duan, S.; Wang, L.; Jia, P.; Zhang, S. Enhancing electronic nose performance based on a novel QPSO-KELM model. *Sensors* **2016**, *16*, 520. [CrossRef] [PubMed]
16. Arshak, K.; Moore, E.; Lyons, G.M.; Harris, J.; Clifford, S. A review of gas sensors employed in electronic nose applications. *Sens. Rev.* **2004**, *24*, 181–198. [CrossRef]
17. Li, Q.; Gu, Y.; Jia, J. Classification of multiple Chinese liquors by means of a QCM-based e-nose and MDS-SVM classifier. *Sensors* **2017**, *17*, 272. [CrossRef] [PubMed]
18. Cavallari, M.; Izquierdo, J.; Braga, G.; Dirani, E.; Pereira-da-Silva, M.; Rodríguez, E.; Fonseca, F. Enhanced sensitivity of gas sensor based on poly (3-hexylthiophene) thin-film transistors for disease diagnosis and environment monitoring. *Sensors* **2015**, *15*, 9592–9609. [CrossRef] [PubMed]
19. Abdallah, S.A.; Al-Shatti, L.A.; Alhajraf, A.F.; Al-Hammad, N.; Al-Awadi, B. The detection of foodborne bacteria on beef: The application of the electronic nose. *SpringerPlus* **2013**, *2*, 1–9. [CrossRef] [PubMed]
20. Capelli, L.; Taverna, G.; Bellini, A.; Eusebio, L.; Buffi, N.; Lazzeri, M.; Guazzoni, G.; Bozzini, G.; Seveso, M.; Mandressi, A.; et al. Application and uses of electronic noses for clinical diagnosis on urine samples: A review. *Sensors* **2016**, *16*, 1708. [CrossRef] [PubMed]
21. Korposh, S.O.; Takahara, N.; Lee, S.W.; Kunitake, T. Fabrication of optical gas sensors using porphyrin-based nano-assembled thin films: A Comparison with bulk materials. In Proceedings of the 2007 7th IEEE International Conference on Nanotechnology (IEEE-NANO), Hong Kong, China, 2–5 August 2007; pp. 1037–1040. [CrossRef]
22. Semeano, A.T.S.; Maffei, D.F.; Palma, S.; Li, R.W.C.; Franco, B.D.G.M.; Roque, A.C.A.; Gruber, J. Tilapia fish microbial spoilage monitored by a single optical gas sensor. *Food Control* **2018**, *89*, 72–76. [CrossRef] [PubMed]
23. Matsumoto, T.; Fukuda, K.; Sugano, K.; Matsumoto, J.; Yasuda, M.; Fueda, Y.; Shiomori, K. Improvement of UV-stability of porphyrin-type humidity indicator by the addition of UV-absorbents. *Kagaku Kogaku Ronbunshu* **2017**, *43*, 123–128. [CrossRef]
24. Guesmi, A. New fluoro triazol porphyrin-cellulose: Synthesis, characterization and antibacterial activity. *Polym. Adv. Technol.* **2016**, *27*, 1517–1522. [CrossRef]
25. Kantar, C.; Akal, H.; Kaya, B.; Islamolu, F.; Türk, M.; Şaşmaz, S. Novel phthalocyanines containing resorcinol azo dyes; Synthesis, determination of pKa values, antioxidant, antibacterial and anticancer activity. *J. Organomet. Chem.* **2015**, *783*, 28–39. [CrossRef]
26. Kalimuthu, P.; Sivanesan, A.; John, S.A. Fabrication of optochemical and electrochemical sensors using thin films of porphyrin and phthalocyanine derivatives. *J. Chem. Sci.* **2012**, *124*, 1315–1325. [CrossRef]
27. Capuano, R.; Pomarico, G.; Paolesse, R.; Di Natale, C. Corroles-porphyrins: A teamwork for gas sensor arrays. *Sensors* **2015**, *15*, 8121–8130. [CrossRef] [PubMed]
28. Tonezzer, M.; Quaranta, A.; Maggioni, G.; Carturan, S.; Mea, G.D. Optical sensing responses of tetraphenyl porphyrins toward alcohol vapours: A comparison between vacuum evaporated and spin-coated thin films. *Sens. Actuators B* **2007**, *122*, 620–626. [CrossRef]
29. Wang, N.; Liu, H.; Zhao, J.; Cui, Y.; Xu, Z.; Ye, Y.; Kiguchi, M.; Murakoshi, K. Theoretical investigation on the electron transport path through the porphyrin molecules and chemisorption of CO. *J. Phys. Chem. C* **2009**, *113*, 7416–7423. [CrossRef]
30. Kladsomboon, S.; Lutz, M.; Pogfay, T.; Puntheeranurak, T.; Kerdcharoen, T. Hybrid optical-electrochemical electronic nose system based on Zn-porphyrin and multi-walled carbon nanotube composite. *J. Nanosci. Nanotechnol.* **2012**, *12*, 5240–5244. [CrossRef] [PubMed]
31. Mensing, J.P.; Wisitsoraat, A.; Tuantranont, A.; Kerdcharoen, T. Inkjet-printed sol-gel films containing metal phthalocyanines/porphyrins for opto-electronic nose applications. *Sens. Actuators B* **2013**, *176*, 428–436. [CrossRef]
32. Jaisutti, R.; Osotchan, T. An investigation of molecular interactions between zinc phthalocyanine thin film and various oxidizing gases for sensor applications. *Adv. Mater. Res.* **2012**, *403–408*, 48–81. [CrossRef]
33. Liu, C.J.; Shih, J.J.; Ju, Y.H. Surface morphology and gas sensing characteristics of nickel phthalocyanine thin films. *Sens. Actuators B* **2004**, *99*, 344–349. [CrossRef]
34. Sugumaran, S.; Jamlos, M.F.; Ahmad, M.N.; Bellan, C.S.; Sivaraj, M. Thickness and annealing effects on thermally evaporated InZnO thin films for gas sensors and blue, green and yellow emissive optical devices. *Opt. Mater.* **2016**, *58*, 342–352. [CrossRef]

35. Wang, B.; Zuo, X.; Wu, Y.; Chen, Z.; He, C.; Duan, W. Comparative gas sensing in copper porphyrin and copper phthalocyanine spin-coating films. *Sens. Actuators B* **2011**, *152*, 191–195. [CrossRef]
36. Long, J.; Xu, J.; Yang, Y.; Wen, J.; Jia, C. A colorimetric array of metalloporphyrin derivatives for the detection of volatile organic compounds. *Mater. Sci. Eng. B Solid* **2011**, *176*, 1271–1276. [CrossRef]
37. Zetola, N.M.; Modongo, C.; Mathlagela, K.; Sepako, E.; Matsiri, O.; Tamuhla, T.; Mbongwe, B.; Martinelli, E.; Sirugo, G.; Paolesse, R.; et al. Identification of a large pool of microorganisms with an array of porphyrin based gas sensors. *Sensors* **2016**, *16*, 466. [CrossRef] [PubMed]
38. Haugen, J.E.; Rudi, K.; Langsrud, S.; Bredholt, S. Application of gas-sensor array technology for detection and monitoring of growth of spoilage bacteria in milk: A model study. *Anal. Chim. Acta* **2006**, *565*, 10–16. [CrossRef]

Analytical Methods

ROYAL SOCIETY OF CHEMISTRY

PAPER

View Article Online
View Journal

Cite this: DOI: 10.1039/d0ay01255f

A hybrid electronic nose system for discrimination of pathogenic bacterial volatile compounds

Thara Seesaard, [a] Chadinee Thippakorn, [b] Teerakiat Kerdcharoen[c] and Sumana Kladsomboon *[d]

A hybrid electronic nose comprising an array of three organic–inorganic nanocomposite gas sensors [zinc tetra *tert*-butyl phthalocyanine (ZnTTBPc), zinc tetra-phenyl porphyrin (ZnTPP), and cobalt tetraphenylporphyrin (CoTPP)] coupled with three commercial metal-oxide semiconductor gas sensors (TGS 2444, TGS 2603 and TGS 2620) was developed to discriminate bacterial volatile compounds. Each type of gas sensor had its own strengths and weaknesses in terms of its capability to detect complex odors from the five different bacterial species tested. Bacterial samples were controlled at a fixed initial bacterial concentration by measuring the optical density at 600 nm of the culture suspensions. A comparative evaluation of the volatile compound fingerprints from five bacterial species grown in Luria–Bertani medium was conducted to identify the optimal incubation time for detection of volatile biomarkers to discriminate among bacteria. The results suggest that the hybrid electronic nose was indeed able to discriminate among the bacterial species and culture media, with a variance based on contributions of 92.4% from PC1 and 7.2% from PC2, at an incubation time of 6 hours. Furthermore, the results of hierarchical cluster analysis showed that bacterial odor data formed two major bacterial groups, with the maximum cluster distance close to 25. Intra-group similarity was demonstrated as the two bacterial species (*E. cloacae* and *P. aeruginosa*) from among the Gram-negative bacteria had a greater similarity with a cluster distance close to 4. Finally, the minimum distance between *E. cloacae* and *S.* Typhi was approximately 1, at an equal distance from *E. coli* and *S. aureus*.

Received 29th June 2020
Accepted 6th November 2020

DOI: 10.1039/d0ay01255f

rsc.li/methods

1. Introduction

Bacterial infection is one of the most important human health problems. It can not only happen more often in people with pre-existing illnesses, but can also occur in a healthy person. Most species of pathogenic bacteria are found as contaminants in the environment, such as in recreational water,[1] slum areas[2] and industrial lands.[3] Bacterial pathogens are often spread through urine and feces. They may infect the skin and underlying soft tissue, as does *Staphylococcus aureus*.[4] There are several types of Gram-negative pathogenic bacteria, including *Pseudomonas aeruginosa* (*P. aeruginosa*), *Escherichia coli* (*E. coli*), *Enterobacter cloacae* (*E. cloacae*) and *Salmonella* Typhi (*S.* Typhi). For example, *P. aeruginosa* can cause opportunistic human infections such as septicemia and pneumonia,[5] and *E. coli* can cause serious food poisoning or toxicity.[6] *E. cloacae* can cause urinary tract infection or pneumonia,[7] while *S.* Typhi causes gastrointestinal infection.[8]

The rapid and accurate identification of the cause of an illness is considered the heart of disease diagnosis. The detection of pathogenic organisms allows intervention to prevent or limit tissue invasion. The precise identification of bacterial species is extremely important in patients because it guides to the most appropriate treatment. Many researchers have tried to develop methods for the early detection of pathogenic bacteria.[9] Using traditional approaches, the identification of bacterial species takes an average of 16–72 hours with techniques such as bacterial culturing,[8] molecular methods,[10] microscopic observation[11] and biochemical testing.[12] Microbiological culturing is one of the primary diagnostic methods in microbiology.[12] Bacterial culturing of body fluids from patients and from environmental specimens remains the gold standard in the diagnosis of most bacterial infections.[13] A revolutionary method, matrix-assisted laser desorption/ionization-time of flight mass spectrometry (MALDI-TOF MS)[14] provides the rapid identification of bacteria and is now popular in advanced clinical laboratories. However, some of these identification methods have not been entirely successful for some bacterial strains. Furthermore, in some remote areas acquiring expensive

[a]*Department of Physics, Faculty of Science and Technology, Kanchanaburi Rajabhat University, Kanchanaburi, 71190, Thailand*

[b]*Center for Research and Innovation, Faculty of Medical Technology, Mahidol University, Phutthamonthon, Nakhon Pathom, 73170, Thailand*

[c]*Department of Physics, Faculty of Science, Mahidol University, Bangkok, 10400, Thailand*

[d]*Department of Radiological Technology, Faculty of Medical Technology, Mahidol University, Phutthamonthon, Nakhon Pathom, 73170, Thailand. E-mail: sumana.kla@mahidol.edu; Tel: +66-89-119-4147*

equipment is not possible. But for laboratories conducting high-throughput detection (*e.g.*, a daily analysis of at least 100 strains), it can be considered a very cost-effective investment.

The development of one alternative method to identify bacterial species has been conducted based on detection of bacterial volatile organic compounds (VOCs).[15] In recent decades, the application of the gas chromatography-mass spectrometry (GC-MS) technique combined with special statistical approaches has been proposed to identify specific bacterial VOC profiles.[16] As summarized in Table 1, many studies have found that there are seven groups of VOCs that are released during bacterial growth, namely, volatile sulfur compounds (VSCs), aldehydes, acids, ketones, hydrocarbons, alcohols and volatile nitrogen compounds (VNCs).[17,18] These growth stage-specific volatile compounds have profiles which are distinct for different species of bacteria. For example, VSCs, aldehydes, acids, ketones, hydrocarbons, alcohols and VNCs are normally produced by *P. aeruginosa*, while ketones and alcohols are observed with *E. cloacae*.[16,19,20] Thus, four species of Gram-negative bacteria and one species of Gram-positive bacteria can produce unique VOC profiles (see Table 1). Although the GC/MS technique is a non-invasive diagnostic tool, the method is complex and the hardware is expensive.[21] Thus, the development of bacterial identification tools, which are accurate, rapid, easy to use and cost-effective, is very challenging.

In recent decades, researchers have revealed that an electronic nose is considered to be a non-invasive tool to assess bacterial volatile compounds using gas sensor arrays.[22] An electronic nose (e-nose) system was reported which used an array of highly sensitive metal-oxide semiconductor (MOS) gas sensors for classification of bacteria into groups. This was based on the class and growth phase of three potentially pathogenic micro-organisms, *E. coli*, *S. aureus* and *Klebsiella oxytoca* (*K. oxytoca*).[23,24] Moreover, a multisensory bacterial volatile compound (BVC) detection system is widely used in the food industry for the detection and monitoring of bacterial contamination.[25] Recent publications have reported the development of e-nose instruments based on measures obtained from multiple sensors in the design of hybrid systems. Examples include MOS sensors combined with GC/MS,[26] metal–organic frameworks combined with MOS sensors,[27] a quartz crystal microbalance (QCM) combined with MOS sensors[28] and a metal oxide semiconductor field effect transistor (MOSFET) combined with MOS sensors.[29] These hybrid gas-sensor array systems have good sensitivity and the ability to detect VOCs and other gases, providing a wide range of possible applications.

Table 1 The normalized concentrations of VOCs from bacteria in culture media

	Gram-negative				Gram-positive
VOC	*E. cloacae*	*E. coli*	*P. aeruginosa*	*S.* Typhi	*S. aureus*
Volatile sulfur compounds (VSCs)					
Dimethyl sulfide, hydrogen sulfide and methyl mercaptan	N/A	6–100[a] (ref. 17 and 18)	17–100[a] (ref. 18)	N/A	59–91[a] (ref. 18)
Aldehydes					
Acetaldehyde, butanal, formaldehyde and 3-methylbutanal	N/A	≈6[a] (ref. 17 and 18)	≈93[a] (ref. 18)	N/A	≈53[a] (ref. 18)
Acids					
Acetic acid and isovaleric acid	N/A	N/A	5–25[b] (ref. 38)	5–25[b] (ref. 38)	≈100[a] (ref. 19), 25–100[b] (ref. 38)
Ketones					
Acetone, 2-cyclopentenone and 2-pentanone	15–20[b] (ref. 20)	≈9[a] (ref. 17)	1–16[b] (ref. 20 and 38)	5–25[b] (ref. 38)	5–25[b] (ref. 38)
Hydrocarbons					
1-Undecene and isoprene	N/A	N/A	≈ 21[a] (ref. 16 and 19), 16–17[b] (ref. 20)	N/A	N/A
Alcohols					
Methanol, ethanol, propanol and 1-butanol	40–100[b] (ref. 20)	1–16[a] (ref. 17, 18 and 39), 5–25[b] (ref. 38)	≈30[a] (ref. 17–19), 25–100[b] (ref. 38)	5–25[b] (ref. 38)	0[a] (ref. 18, 19 and 40), 5–25[b] (ref. 38)
Volatile nitrogen compounds (VNCs)					
Ammonia, acetonitrile, hydrogen cyanide, trimethylamine, indole and 2-aminoacetophenone	N/A	0–6[a] (ref. 18, 40 and 41), 25–100[b] (ref. 38)	0–58[a] (ref. 17–19), 1–25[b] (ref. 38)	1–25[b] (ref. 38)	≈3[a] (ref. 17), 1–5[b] (ref. 38)

[a] Normalization using the min–max normalization $[100 \times ((X_i - X_{Minimum}) \times (X_{Maximum} - X_{Minimum})^{-1})]$, where X is the concentration of VOCs.[42] [b] Normalization using the internal standard (IS) N/A = not available.

There are many kinds of systems that can detect bacterial volatile compounds to a certain extent and do not require Gram staining for identification. But these methods often do not consider the impact of such variables as temperature and stage of the bacterial growth cycle, and so these methods cannot be applied in the medical field as a scanning tool to detect the smell of bacteria growing on or in the body.

At present, there are no reports demonstrating selectivity using organic–inorganic nanocomposite gas sensors coupled with MOS gas sensors in a hybrid e-nose system. Recently, advances have been made with a new method, differential mobility spectrometry (DMS) classification of bacteria.[30]

It successfully classifies all bacterial species and distinguishes Gram status. The publication of this research has yielded many useful rapid bacterial identification technologies, allowing timely initiation of the most appropriate therapy. However, the sensor has limitations in distinguishing bacteria of the same genus. At present, there are no reports demonstrating selectivity using organic–inorganic nanocomposite gas sensors coupled with MOS gas sensors in a hybrid e-nose system. Therefore, our research work will extend the demonstrated functionality of electronic sensing technology beyond the existing landscape. Moreover, our system is aimed at utilizing consumer electronics which are available, affordable and easy-to-use. In this research, we developed a hybrid e-nose system which utilizes two types of gas sensors: (i) three organic–inorganic nanocomposite gas sensors [zinc tetra-*tert*-butyl phthalocyanine (ZnTTBPc), zinc tetra-phenyl porphyrin (ZnTPP), and cobalt tetraphenyl-porphyrin (CoTPP)], coupled with (ii) three MOS gas sensors (TGS 2444, TGS 2603 and TGS 2620). These organic dyes, namely metallo-porphyrin (MP) and metallo-phthalocyanine (MPc), are frequently used as gas sensors based on optical sensing principles because they have delocalized π-systems. These are proven to have high performance as electron transport materials that leads to changes in their optical properties.[31] Recently, organic–inorganic dyes were used as sensor materials forming an integral part of an optical gas sensing system for classification of bacterial species.[32] However, low electrical conductivity of organic–inorganic dyes is an issue in the design and fabrication of electrical gas sensors. The efficiency of electrical conductivity in nanocomposite gas sensors is enhanced by embedding carbon nanotubes (CNTs).[33] In addition, adding CNTs can improve the ability to transfer electrons between the conducting network and VOCs adsorbed onto the sensing surface. The increased aggregate surface area increases the percentage of the sensor response.[32] Thus, nanocomposite gas sensors based on organic–inorganic dyes and carbon nanotubes may detect bacteria and microbial odors in many applications, such as quality control of food products,[34] safety and security,[35] environmental monitoring[36] and medical diagnosis.[37]

The objective of this research was to develop a hybrid e-nose system based on different organic–inorganic materials for bacterial identification. MOS and organic–inorganic based gas sensors were fabricated and installed into the system. This hybrid e-nose system was tested for performance and efficiency on many volatile organic compounds, which represent bacterial volatile compounds such as acetic acid, acetone, ammonia, ethanol, ethyl acetate, formaldehyde and H_2O. In addition, characteristic odors, produced as metabolites of different combinations and quantities of bacteria, were detected and correlated with the Gram stain classification of the bacteria. Five bacterial species, namely *E. coli*, *E. cloacae*, *P. aeruginosa*, *S.* Typhi and *S. aureus*, were distinguished based on their odorants using statistical methods [principal component analysis (PCA) and hierarchical cluster analysis (CA)].

2. Experimental section

2.1. Fabrication of the organic–inorganic dye/multiwall carbon nanotube composite gas sensor

Organic–inorganic dyes, namely zinc-2,9,16,23-tetra-*tert*-butyl-29*H*,31*H*-phthalocyanine (ZnTTBPc), zinc-5,10,15,20-tetraphenyl-21*H*,23*H*-porphyrin (ZnTPP) and cobalt-5,10,15,20-tetraphenyl-21*H*,23*H*-porphine (CoTPP), were purchased from Sigma-Aldrich (St. Louis, MO, USA).

The multiwall carbon nanotubes (MWCNTs) were synthesized using an infusion chemical vapor deposition method from Chiang Mai University.[43] First, ZnTTBPc, ZnTPP and CoTPP were dissolved in a chloroform solution at a concentration of 5 mg ml^{-1} to prepare organic–inorganic dye solutions, while MWCNTs were dispersed in chloroform by means of sonication at a concentration of 2 mg ml^{-1}. Then the MWCNT solution was blended into each organic–inorganic dye solution in order to obtain high electrical conductivity with a ratio of percent loading for the MWCNT solution to dye solution of 50 : 50. Each organic–inorganic dye solution, with MWCNTs dispersed in it, was stirred for 15 min, followed by 30 min of continuous ultrasonic vibration at 25 °C. This was repeated three times to ensure uniformity and homogeneity. [The molecular structures of ZnTTBPc, ZnTPP and CoTPP are shown in Fig. 1(a)]. Finally, three organic–inorganic dye/multiwall carbon nanotube composite mixtures (*i.e.* ZnTTBPc/MWCNT, ZnTPP/MWCNT and CoTPP/MWCNT solutions) were spin-coated onto interdigitated Cr/Au electrodes at 1000 rpm for 30 seconds to produce gas sensor devices, as shown in Fig. 1(b). The interdigitated electrodes (IDEs) were fabricated by E-beam evaporation of Cr/Au thin films deposited on alumina substrates.[44] The thicknesses of the Cr and Au film layers were 50 nm and 200 nm, respectively. The IDEs were an important component of the organic–inorganic dye/MWCNT gas sensor, functioning as the sensing area (the surface area was approximately 0.1×1 mm^2).

2.2. Metal-oxide semiconductor gas sensors

Three commercial metal-oxide semiconductor (MOS) gas sensors, namely TGS 2444, TGS 2603 and TGS 2620, were purchased (Figaro USA Inc., IL, USA). These MOS gas sensors respond to the VOCs in each target gas and other hazardous organic compounds.[45,46] The metal oxide gas sensing materials used with n-type metal oxide semiconductors for bacterial gas sensing are tin oxide (SnO_2)[47] and tungsten trioxide (WO_3).[48] The structures of the single sensing elements are comprised of

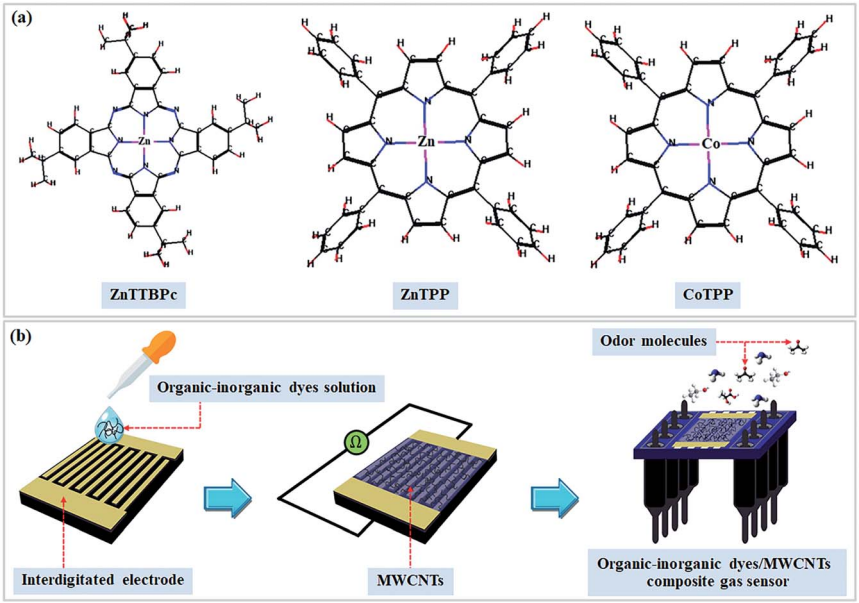

Fig. 1 (a) Structures of ZnTTBPc, ZnTPP and CoTPP, and (b) the fabrication process of the organic–inorganic dye/MWCNT composite gas sensor.

a metal oxide semiconductor layer formed on the alumina substrate of a sensing chip together with an integrated heater. After applying a heating voltage, reducing or oxidizing gases are applied to the sensing layer. The electrical resistance (R) of MOS-type gas sensors changes due to the change in adsorbed oxygen concentration.[48]

2.3. Testing of the hybrid gas sensor arrays

The details of the gas sensor arrays used in our hybrid electronic nose system are listed in Table 2. Organic–inorganic nanocomposite gas sensors can operate in a room-temperature environment, while the MOS gas sensors commonly operate at a high temperature, ranging from 150 °C to 400 °C which requires a heating element. TGS 2444 was highly selective for ammonia gas and had some response to hydrogen sulfide.[45] TGS 2603 was sensitive to low concentrations of the amine-series, air contaminants, and sulfurous vapors, such as trimethyl amine, hydrogen sulfide, hydrogen and ethanol (ethyl alcohol).[46] TGS 2620 was highly selective for general organic solvents such as alcohol, methanol and carbon monoxide.[46] In addition, organic–inorganic dye/multiwall carbon nanotube (MWCNT) composite gas sensors, namely ZnTTBPc/MWCNT, ZnTPP/MWCNT and CoTPP/MWCNT, were used for detection of general organic solvents such as alcohol, acetone, and acetic acid.[32,49]

In this study, the sensitivity and selectivity of gas sensors were tested with acetic acid, acetone, ammonia, ethanol, ethyl acetate, formaldehyde and H_2O. These VOCs have been considered sensitive and specific biomarkers for bacteria. The seven volatile organic compounds were purchased from Merck KGaA (USA), while pure air (zero air) was purchased from Rungcharoen Oxygen Co., Ltd. (Bangkok, Thailand). The details of VOC preparation for testing are shown in Table 3. The number of gas molecules contained in one cubic meter of an ideal gas can be calculated using Loschmidt's number.[50] In addition, the volume of each VOC solution at a concentration of 1000 ppm was calculated based on its molecular weight (MW) and density. A VOC solution was injected into a 1000 ml glass bottle that was placed in a temperature-controlled water bath at the evaporating temperature of that VOC. Each VOC was evaporated at a temperature from 25 °C to 100 °C which was related to its boiling point. Moreover, an zero air carrier system was

Table 2 Details of the gas sensor arrays used in the hybrid electronic nose system

Code	Sensor class	Sensor type (target compounds)	Detection range (ppm)
S1	ZnTTBPc/MWCNT	Nanocomposite gas sensor (organic solvents)	>902[a]
S2	ZnTPP/MWCNT	Nanocomposite gas sensor (organic solvents)	>515[a]
S3	CoTPP/MWCNT	Nanocomposite gas sensor (organic solvents)	>2433[a]
S4	TGS 2444	MOS (ammonia and hydrogen sulfide)	166[a], 10–300[b] (ref. 45)
S5	TGS 2603	MOS (amine-series and sulfurous vapors)	>236[a], 1–10[b] (ref. 46)
S6	TGS 2620	MOS (alcohol and organic solvents)	>141[a], 50–5000[b] (ref. 46)

[a] Typical detection range obtained from the study (see Table 4). [b] Typical detection range was reported by manufacturers of Figaro gas sensors.

Table 3 Preparation of VOCs at a concentration of 1000 ppm in pure air

VOC	Evaporating temperature[a] (°C)	MW (g mol^{-1})	Density (g ml^{-1})	Volume of VOC solution in cylinder (μl)
Acetic acid (35%)	100	60.05	1.05	2.60
Acetone (100%)	56	58.08	0.79	3.29
Ammonia (29%)	25	17.03	0.91	0.84
Ethanol (100%)	78	46.07	0.79	2.62
Ethyl acetate (100%)	77	88.11	0.90	4.38
Formaldehyde (37%)	25	30.03	1.09	1.24
H_2O (100%)	100	18.02	1.00	0.81

[a] Evaporating temperature depends on the boiling point of each VOC.

installed inside the system to spread the VOC's vapor evenly across the bottle and deliver it to the sensor chamber. Then, the resistances of both the sensors were measured; the experiment was repeated three times to obtain a consistent dimension.

2.4. Design of the hybrid electronic nose system

The hybrid electronic nose system was designed in a briefcase form so it could be carried or easily moved. The system consisted of three main components: (i) the gas sensor array unit, (ii) odor-delivery unit, and (iii) data acquisition (DAQ) unit [shown in Fig. 2(a)]. In the gas sensor array unit, there were six different types of gas sensors (Table 2). Three MOS gas sensors and three organic–inorganic dye/MWCNT nanocomposite gas sensors were installed into the sides of the octagon-shaped chamber which was made of Teflon (PTFE) to prevent the VOCs from sticking to the chamber. A schematic of the chamber structure provides two views: the top view and side view [Fig. 2(b)]. The center of the bottom plate of the sensor chamber was pierced to make a gas inlet hole for delivering odors to the electronic nose.

The odor-delivery unit had a solenoid valve for switching between the odor sample (target odor) and zero air (reference gas) for gas delivery into the sensor chamber. Zero air, produced by mixing pure oxygen with pure nitrogen (21% oxygen and 79% nitrogen), was purchased from the gas industry (Rungcharoen Oxygen Co., Ltd., Bangkok). In the olfactory sensitivity testing, zero air (pure air) was used as the carrier gas to deliver the odor sample into the sensor chamber of the hybrid e-nose system. In addition, any background odors contained in the chamber were expelled by zero air flushing. Flow meters were used to monitor the flow rate of the pure air stream in real time so it could be controlled to 400 ml min^{-1}. A data acquisition card (NI USB-6008 of National Instruments, Singapore) with LabVIEW software was installed on a computer and used to convert the analog voltage into a digital signal. Then, the resistance change of each gas sensor was calculated based on a voltage divider concept and sent to the computer.

2.5. Bacterial odor measurement and data processing

Fig. 3 shows a schematic diagram of the hybrid e-nose system for bacterial odor-sensing using two distinct types of gas sensors. In order to test the chemical sensing of the hybrid e-nose, dynamic flow measurements were conducted by switching between the bacteria's odor sample for 2 min and pure air (zero air) for 3 min. This process was repeated for 4 cycles. The temperature was controlled at around 37 °C for bacterial samples and at evaporation temperatures (see in Table 3) for VOC samples. The base-line resistance and the changing

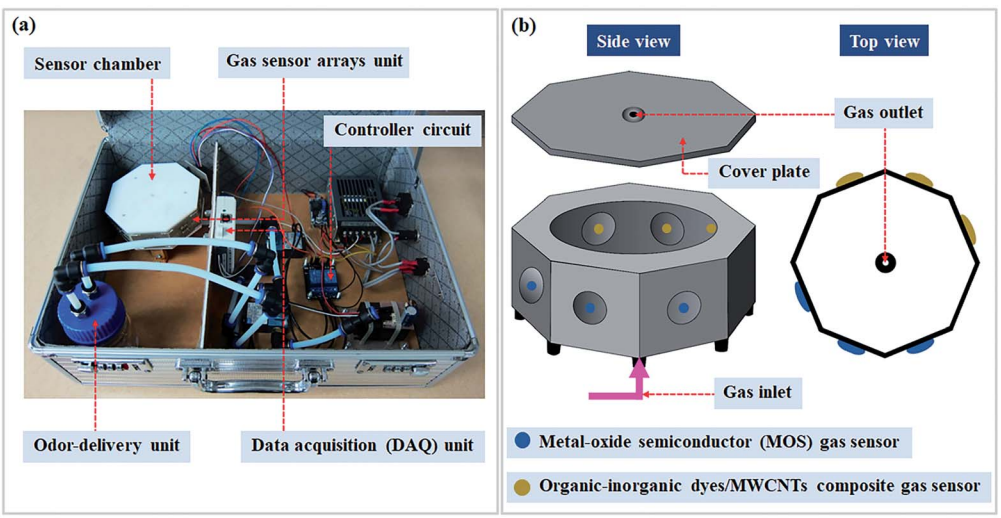

Fig. 2 (a) The physical structure of the hybrid electronic nose system and (b) the schematic of the chamber structure; top view and side view.

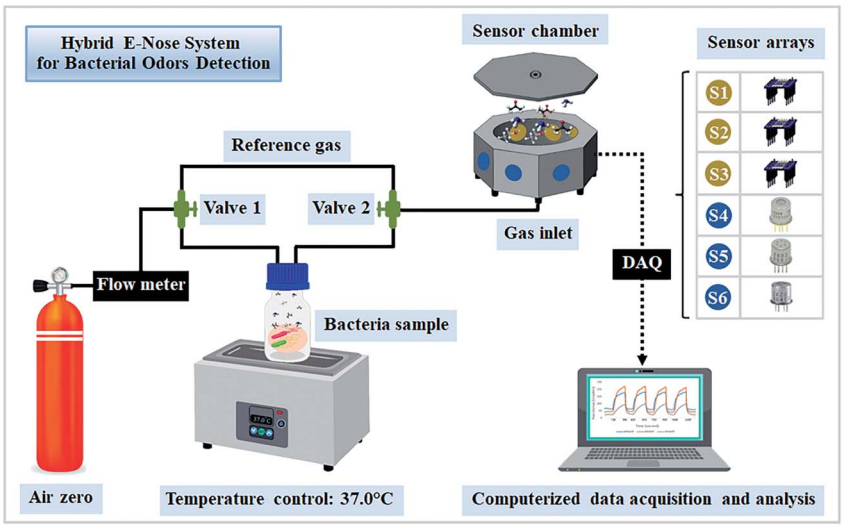

Fig. 3 Schematic diagram of the hybrid e-nose system for detection of bacterial odors.

resistance with time of the gas sensors were recorded every 1 second. The sensor response from each of the six sensors is defined as the difference between the maximum resistance-change (the resistance change upon absorption of the sensed gas) and the baseline resistance (the resistance from zero air). These responses from the sensor arrays were then analyzed based on pattern recognition by principal component analysis, a simple and effective method to recognize patterns in the data by visualizing them in 2-dimensional or 3-dimensional plots.[51] Each experiment was confirmed by analyzing bacterial odor information using a combination of principal component analysis and hierarchical cluster analysis (CA).[52]

The sensor response (S) from each of the six gas sensors was described as the sensitivity of a gas sensor to different gases. Sensitivity (%) was defined by eqn (1) as follows:

$$\text{Sensitivity } (\%) = \frac{\Delta R}{R_0} \times 100 \quad (1)$$

where R_0 is the initial resistance of each sensor without the sample vapor (baseline resistance) and ΔR is the difference in resistance detected by the sensor between the bacterial odor and pure air.

2.6. Bacterial sample preparation

The five bacterial pathogens investigated in this study were *Enterobacter cloacae* subsp. *cloacae* (ATCC 13047), *Staphylococcus aureus* subsp. *aureus* (ATCC 29213), *Escherichia coli* (ATCC 25244), *Pseudomonas aeruginosa* (ATCC 27853) and *Salmonella enterica* subsp. *enterica serovar* Typhi or *S.* Typhi (ATCC 19430). Each of these selected bacteria can cause nosocomial infection, some are found in the natural environment, and all tend to be resistant to disinfectants and antibiotics. The strains were obtained from the Faculty of Medical Technology, Mahidol University, Thailand. Briefly, the bacteria were grown in sterile nutrient media at 37 °C for cell recovery and then single isolated colonies were sub-cultured in Luria–Bertani (LB) liquid medium at 37 °C in a shaking incubator (180 rpm) for 9 h. Cloudy media after cultivation were observed and measured for bacterial growth characteristics. The initial concentration of bacteria was determined using optical density (at 600 nm). Bacterial growth cultures were optimized and adjusted until an OD600 of 0.3 was reached. Then, a batch culture was prepared by transferring 25 μl of each bacterial culture into 25 ml of LB broth to control the initial bacterial number in the sample bottles for odor detection.

These bacterial cultures were then grown at a constant incubation temperature (IT) of 37 °C. Culture samples were removed at intervals and the number of viable bacteria was counted *via* the increasing turbidity as observed at OD600. A logarithmic growth curve for each bacterial strain was plotted. Finally, the OD600 value and gas sensing response to each bacterial culture were collected every 3 hours.

3. Results and discussion

3.1. Bacterial growth curve analysis

The growth phase of five bacterial species in liquid culture media was measured using the optical density at 600 nm (OD600) of the culture suspensions with a UV-visible spectrophotometer. The initial cell concentration of the five bacterial species was standardized by using the same value of optical density (OD600 nm). The growth curve of the bacteria was plotted by measuring OD600 values from 0 to 12 h incubation (Fig. 4).

Growth curves were obtained using the polynomial regression equation, *i.e.* $Y = A_1 + (A_2 + A_1)(1 + 10^{[(\log X_0 - X) \times P]})$, where X is time, Y is optical density and A_1, A_2, and P are constant values. The cell density of all cultures increased slightly during the first 2 h of incubation and then rapidly during hours 3–8. The stationary phases (no further increase in cell density) of the five bacterial species were observed after 9 h of incubation. There was a different logarithm of living bacterial cells for each of the

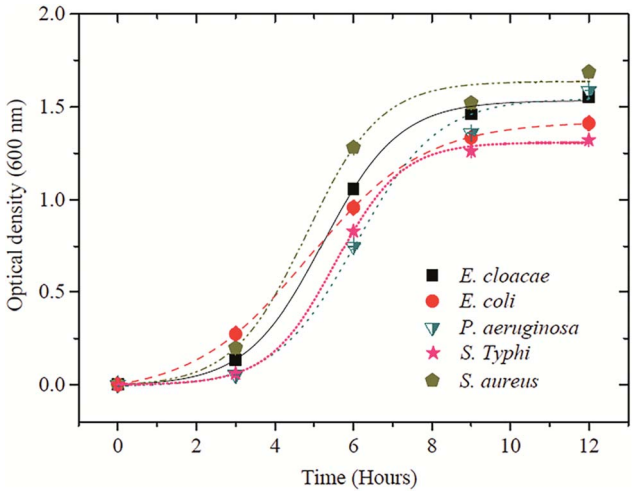

Fig. 4 The optical densities of *E. cloacae*, *E. coli*, *P. aeruginosa*, *S. aureus* and *S.* Typhi in liquid culture media were obtained in triplicate samples.

five pathogens, and each had a high R-squared (R^2) value. At the exponential (log) phase (6 h incubation), *S. aureus* had the greatest cell density when compared with those of *E. cloacae*, *E. coli*, *S.* Typhi and *P. aeruginosa* (the coefficient of determination; R^2 values of 0.99415, 0.99857, 0.99998, 0.99929 and 0.99003, respectively). A typical four-phase pattern of bacterial growth was seen in this study for each species. However, *S. aureus* and *E. cloacae* entered log phase growth quicker than *E. coli*, *S.* Typhi and *P. aeruginosa* which each displayed a prolonged lag period.[20] The unique growth behaviors of different pathogens might have been related to species-specific odor-releasing processes.

3.2. Sensor performance and calibration at elevated VOC concentrations

In order to evaluate the performance of the self-built hybrid e-nose system for bacterial identification, seven volatile organic compounds (VOCs), produced by bacteria as waste products, were selected to further evaluate the sensor performance based on sensitivity and specificity. Specifically, acetic acid, acetone, ammonia, ethanol, ethyl acetate, formaldehyde and H_2O at a concentration of 1000 ppm were utilized in the assessment.

In analytical chemistry, researchers calculate the limit of detection (LOD)[53]: the smallest amount or concentration of an analyte gas in the test sample that can be reliably distinguished from pure air or the blank. The LODs of seven VOCs with six different gas sensors are presented in Table 4. The LOD is defined according to eqn (2) as follows:

$$\mathrm{LOD} = 3 \times \frac{\mathrm{SD_{blank}}}{\mathrm{slope}} \quad (2)$$

where SD_{blank} is the standard deviation of the blank signal (or sensor signal under pure air flow) and *slope* is the slope of the sensitivity curve which is measured in the concentration range of 1000–3000 ppm. The concentration of each VOC was measured three times to check reproducibility.

Choosing the most appropriate gas sensors for detection of each bacterial odor used volatile testing in the dynamic system in order to achieve optimal detection and sensitivity of each sensor. It was found that six hybrid gas sensor arrays, three organic–inorganic nanocomposite gas sensors (ZnTTBPc, ZnTPP and CoTPP) coupled with three commercial metal-oxide semiconductor (MOS) gas sensors (TGS 2444, TGS 2603 and TGS 2620), under dynamic gas flow testing showed excellent sensitivity (Fig. 5). The sensitivity for the three organic–inorganic nanocomposite gas sensors was expected to be in the range of approximately 0.002% to 1.41% at 1000 ppm. The three commercial MOS gas sensors had a wide sensitivity range (from 1.86% to 99.03%) as well as a quick response and short recovery time. The MOS gas sensors provided greater sensitivity than the organic–inorganic nanocomposite gas sensors. However, each sensor showed a significantly different pattern of specific volatile organic compounds.

Among the organic–inorganic nanocomposite gas sensors, the CoTPP/MWCNT gas sensor (S3) showed the highest sensitivity to ethyl acetate, which is found in volatile bacterial metabolites.[54] The ZnTPP/MWCNT gas sensor (S2) demonstrated a striking response when detecting acetic acid, mainly related to the growth of *P. aeruginosa*, *S.* Typhi and *S. aureus*.[19,38] Moreover, the bar chart (Fig. 5) also shows that water elicited negligible responses from all sensors and so should not have any significant influence on the accuracy of the analytical results.[55] Therefore, we conclude that these sensors, fabricated from porphyrin and phthalocyanine, are well suited for use as sensor arrays for volatile biomarkers in bacterial odors. Among the MOS gas sensors, the TGS 2603 gas sensor (S5) yielded its highest response to acetic acid, and then, in decreasing order, to formaldehyde, ethanol and acetone. The TGS 2620 gas sensor (S6) showed the second highest responses to acetic acid, ethanol and acetone. In contrast, the TGS 2444 gas sensor (S4) showed similar minor responses to all seven VOCs tested. However, inclusion of the full set of sensors (S1–S6) in this hybrid e-nose system was necessary to generate the odor-specific patterns which detected and identified the bacteria-specific odors. Study of the practical considerations in gas sensor performance not only demonstrates excellent sensitivity and outstanding selectivity to the target gas molecules, but also the stability after being used for a long time. Long-term stability experiments were conducted on six gas sensors toward pure air (without gas) over a total period of 30 days, as shown in Fig. 6. The standard deviation (SD) of baseline resistance for each of

Table 4 Limit of detection (LOD) of gas sensor arrays for seven VOCs (ppm)

VOCs	S1	S2	S3	S4	S5	S6
Acetic acid	902	578	5713	369	329	174
Acetone	3282	1233	9380	466	1502	339
Ammonia	4108	1041	6075	166	441	152
Ethanol	1297	7362	5786	755	3782	141
Ethyl acetate	1554	515	2433	490	236	164
Formaldehyde	1341	840	10 194	2143	1444	219
H_2O	105 138	96 284	243 550	583	2225	345

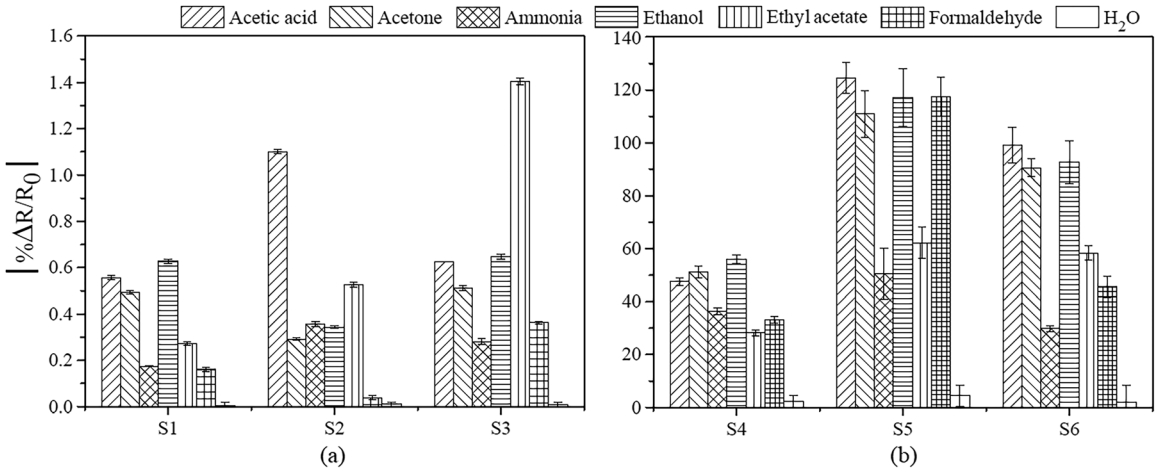

Fig. 5 Average sensitivity (%) for (a) organic–inorganic nanocomposite gas sensors and (b) commercial metal-oxide semiconductor (MOS) gas sensors toward seven VOCs at a concentration of 1000 ppm under dynamic gas flow testing (400 ml min^{-1}).

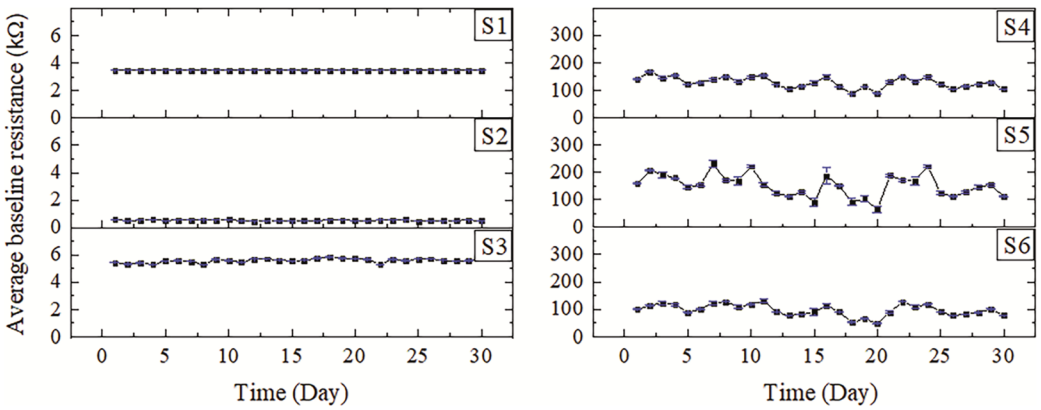

Fig. 6 The relationship between the long-term stability of the baseline resistance and the aging time for three organic–inorganic nanocomposite gas sensors (S1–S3) and three commercial metal-oxide semiconductor (MOS) gas sensors (S4–S6).

the six gas sensors (S1–S6) was 0.05, 6.16, 2.60, 14.98, 27.05 and 22.28%, respectively. It is clearly shown that the SDs of the baseline resistance for the three organic–inorganic nanocomposite gas sensors (S1–S3) were each less than 10% toward pure air, which revealed the great stability of the sensors, while the SDs of the three commercial metal-oxide semiconductor (MOS) gas sensors (S4–S6) were each more than 10% toward pure air, which revealed their poor stability.

3.3. Detection and analysis of bacterial volatile organic compounds

Fig. 7 shows the sensing signals on an organic–inorganic nanocomposite gas sensor (CoTPP/MWCNT; S3) and a commercial metal-oxide semiconductor gas sensor (TGS 2620; S6) recorded as changes in resistance as a function of time of the five types of bacterial odors at 6 h incubation. The dynamic flow measuring was performed by switching between the baseline detection of pure air (zero air) for 3 min and the detection of the sample bacteria's odor for 2 min. This cycle was repeated four times.

After three seconds, we observed an abrupt change in the resistance values of the CoTPP/MWCNT gas sensor (S3) when exposed to each bacterial volatile compound [Fig. 7(a)]. In contrast, for the same samples the resistance values of the TGS 2620 gas sensor (S6) decreased abruptly to reach its lower resistance [Fig. 7(b)]. These results showed that the organic–inorganic nanocomposite gas sensors (S1–S3) were n-type semiconductors, whereas the MOS gas sensors were p-type semiconductors, increasing and decreasing the resistivity under oxidizing gas conditions.[56] The resistance changes during gas sensing of the two types of gas sensors were different, in accordance with their distinct sensing mechanisms. The differences between the signals from the bacterial odor and pure air (base line) were used as features in the PCA and CA analyses.[51,52]

The ZnTPP/MWCNT (S2) and TGS 2603 (S5) gas sensors were specifically required for detection of acetic acid vapor. This vapor was found at high levels from Gram-positive bacteria (*S. aureus*) but was not found in vapors of two of the Gram-negative bacteria (*E. coli* and *E. cloacae*) (see Table 1). These sensors have

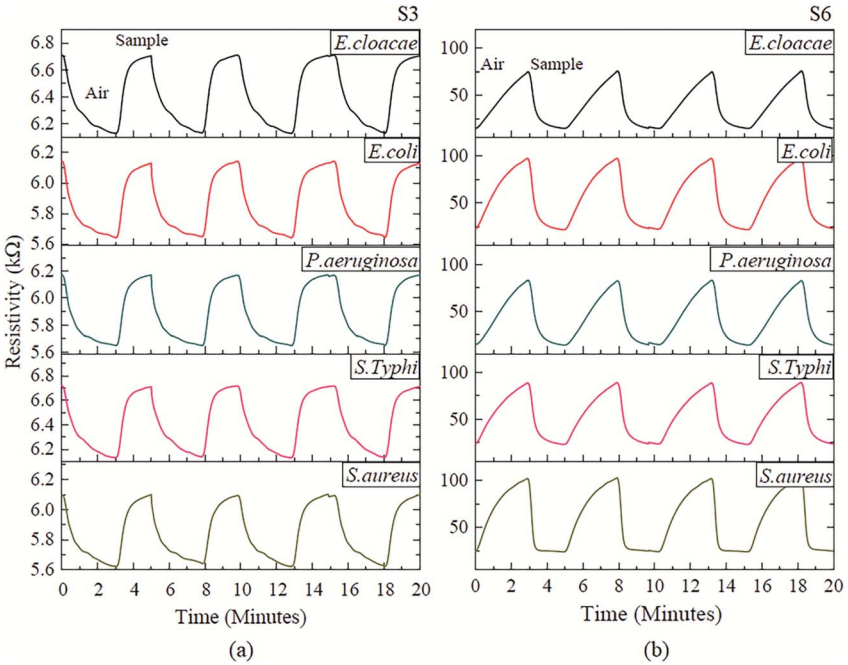

Fig. 7 The sensing signals of the (a) CoTPP/MWCNT gas sensor (S3) and (b) TGS 2620 gas sensor (S6) in response to five types of bacterial odors after 6 h incubation as measured using the self-built hybrid electronic nose.

also been tested with other volatile biomarkers (ammonia, ethyl acetate and water) and were found to have less sensitivity for them.

The graphs in Fig. 5 and 8 show the sensitivities of each sensor (S1–S6) when tested for seven volatile compounds in five bacterial odor samples. It was found that the TGS 2603 (S5) and TGS 2620 (S6) gas sensors were the most sensitive for detecting *E. cloacae* odor. These results were consistent with the amounts of acetic acid, formaldehyde, ethanol, acetone and ethyl acetate forming the volatile constituents of each bacterial odor. In addition, the CoTPP/MWCNT (S3) and ZnTPP/MWCNT (S2) gas sensors demonstrated striking responses when detecting *E. cloacae* and *P. aeruginosa*, respectively.

The *p*-value approach to hypothesis testing with a significance level of 95% was used to compare the sensitivity of each sensor to each bacterial odor from four Gram-negative and one Gram-positive bacterial sample released after 6 h of incubation at 37 °C. Their statistical significances (*p*-value in parentheses) were S1 (0.03), S2 (0.01), S3 (0.00), S4 (0.01), S5 (0.30) and S6 (0.03). This revealed that the TGS 2603 gas sensor (S5) showed no statistically significant difference in its sensitivity to Gram-negative and Gram-positive bacteria. However, the sensitivities

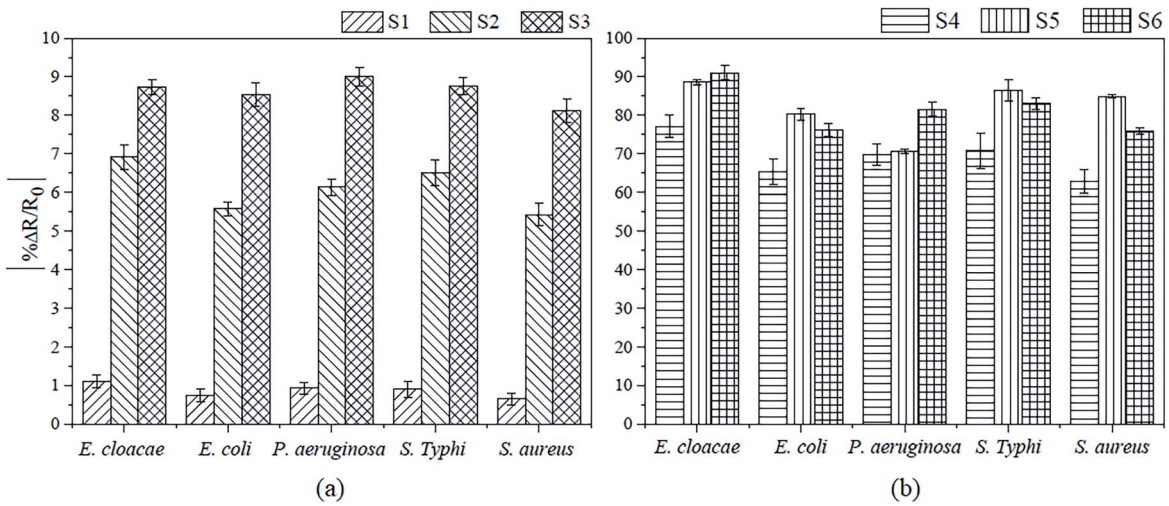

Fig. 8 The sensitivity of the organic–inorganic nanocomposite gas sensors (S1–S3) and the commercial metal-oxide semiconductor gas sensors (S4–S6) obtained upon exposure to volatile biomarkers from five different species of bacteria at an incubation period of 6 h at 37 °C.

of the other five sensors (S1, S2, S3, S4 and S6) were significantly different based on the Gram staining results.

The effect of incubation duration on the bacterial growth and metabolic activity of the five species of pathogenic bacteria, and their yield of volatile biomarkers allowing species discrimination, was investigated through sniffing every 3 h. Principal component discrimination analysis score plots were created in order to find odor patterns which enhanced discrimination. The odors produced by the five species of bacteria (*E. cloacae*, *E. coli*, *P. aeruginosa*, *S.* Typhi and *S. aureus*) and culture media after different lengths of incubation were distinguished and grouped using ellipses based on 95% confidence.[57] The odor patterns shown in Fig. 9(a) and (d) show that the clusters of the five species of bacteria and culture media during the lag (3 h) and stationary (12 h) phases were not clearly separated. This implies that each bacterial sample's odor during these incubation phases had few differences.

Discrimination of odor components was seen at 6 h of incubation of *E. cloacae*, *E. coli*, *P. aeruginosa*, *S.* Typhi and *S. aureus* and culture media (Fig. 9(b)). PC1 and PC2 account for 92.40% and 7.20% of the variance, respectively, which completely separated the odor data of each bacterial species and culture media. Therefore, it seems certain that the results of bacterial odor discrimination were not influenced by culture media odor. The growth curves (see Fig. 4) showed that the 6 h time points occurred during the log phase of the bacterial growth cycles, the time when the cells were dividing and doubling in number. This is the phase when metabolic activity is high, and DNA, RNA, cell wall components, and other substances necessary for growth are generated to support division.[41,58] Therefore, the hybrid e-nose had the ability to identify unique odor patterns associated with each bacterial species when their metabolism made these prominent and thus useful for further diagnostic applications.

Although the bacterial odors from the five species at 9 h of incubation (shown in Fig. 9(c)) were separated into five groups on the PCA plots, they stood quite close to each other on the PCA axis and overlapped with the culture media. PC1 and PC2 contributed 91.9% and 7.6% of the total variance, respectively. As a matter of fact, in the stationary phase the number of dividing cells equals the number of dying cells[59] and results in no overall population growth. The cells become less metabolically active and less volatile biomarkers are released from cultures.[41]

Gram staining helps to differentiate bacterial species, allowing the diagnosis of infections and identification of which species gives a food it's fantastic character. Gram staining is a common technique used to differentiate two large groups of bacteria based on the structure of their cell walls.[60] The two key features that lead to the differentiation of Gram-positive and

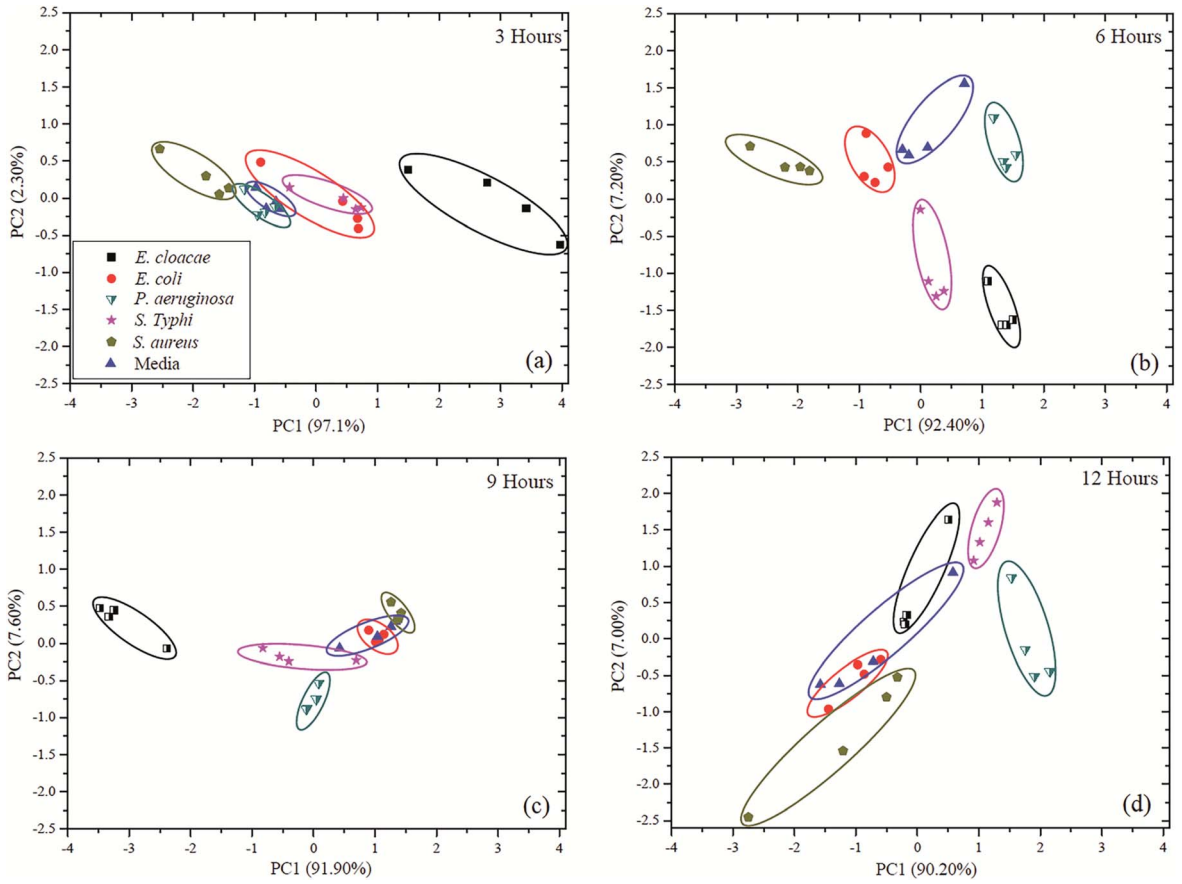

Fig. 9 Schematic diagrams of principal component analysis (PCA) of culture media and five species of pathogenic bacteria in culture media with self-built hybrid e-nose measurements at (a) 3 h, (b) 6 h, (c) 9 h and (d) 12 h incubation times.

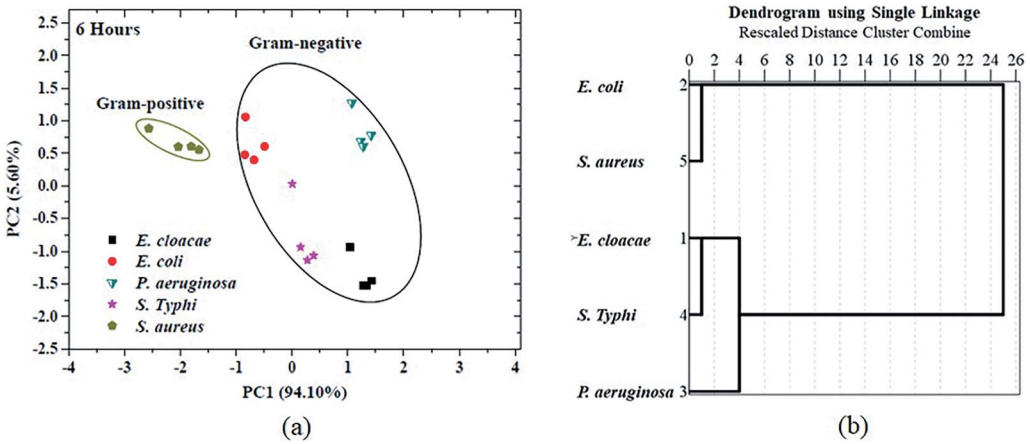

Fig. 10 (a) 2D principal component analysis (PCA) and (b) cluster analysis (CA) performed on bacteria odor data between the Gram-negative group and Gram-positive group.

Gram-negative species are the thickness of the peptidoglycan layer and the presence or absence of an outer lipid membrane.[61] Though both groups of bacteria can cause diseases, their respective treatments differ. For bacterial infections, Gram staining helps determine what kind of medication is needed for the best results. In this research, discrimination between Gram-positive and Gram-negative bacteria may be performed accurately by using the e-nose. Volatile compounds of four Gram-negative and one Gram-positive bacterial species, after 6 h of incubation, were identified and clustered separately using pattern recognition methods based on principal component analysis and hierarchical cluster analysis (Fig. 10).

The results of PCA and CA analyses [shown in Fig. 10(a) and (b)] revealed that the bacterial odor patterns from the group of Gram-negative bacteria (black ellipse) were clearly separated from those of the Gram-positive species (green ellipse), $p < 0.05$. Furthermore, this suggested that some volatile constituents in the bacterial odor of each species were obviously different. The interpretation of the results of CA was that bacterial odor data formed two major groups: odors from *E. cloacae*, *E. coli*, *P. aeruginosa* and *S.* Typhi (all Gram-negative bacteria) and from *S. aureus* (a Gram-positive bacterium). The maximum distance between the two comparative bacterial groups was significantly different.[25] Intra-group similarity was demonstrated as two bacterial odor samples from the Gram-negative group (*E. cloacae* and *P. aeruginosa*) showed a single-linkage (nearest neighbor) distance of close to 4. The minimum distance between *E. cloacae* and *S.* Typhi was approximately 1, which was at an equal distance between *E. coli* and *S. aureus*. Therefore, while the Gram-negative bacterial odors were all different from each other, they were each distinct from the Gram-positive bacterial odor. This was confirmed by analyzing bacterial odor information by a combination of principal component and hierarchical cluster analyses.

4. Conclusions

A self-built hybrid electronic nose prototype which combined three organic–inorganic nanocomposite gas sensors and three commercial metal-oxide semiconductor gas sensors was developed. The three nanocomposite gas sensors were successfully fabricated from a combination of carbon nanotube and organic–inorganic dyes, *i.e.* ZnTTBPc, ZnTPP and CoTPP. The gas sensor arrays provided an acceptable limit of detection and sensitivity when assaying seven volatile organic compounds released from bacterial cultures. Combined with PCA analysis, the hybrid electronic nose discriminated the odors from *E. cloacae*, *E. coli*, *P. aeruginosa*, *S.* Typhi and *S. aureus* (after 6 h of incubation) with 99.7% of the total variance. Based on the CA analysis, four Gram-negative bacteria (*i.e.*, *E. cloacae*, *E. coli*, *P. aeruginosa* and *S.* Typhi) were completely separated from one Gram-positive bacteria (*S. aureus*) with an approximate distance of 25. According to the results, we conclude that this hybrid electronic nose prototype has high potential to identify bacterial species as a non-invasive, pathogenic bacterial monitoring system and has several advantages such as being easy to use, cost effective, rapid and non-destructive.

Conflicts of interest

There are no conflicts to declare.

Acknowledgements

This project was supported by Mahidol University and the Thailand Research Fund (TRF) (Grant No. MRG6080151).

References

1 R. T. Noble and S. B. Weisberg, *J. Water and Health*, 2005, **3**, 381–392.
2 A. Y. Katukiza, M. Ronteltap, P. van der Steen, J. W. A. Foppen and P. N. L. Lens, *J. Applied Microbiology*, 2014, **116**, 447–463.
3 N. Massad-Ivanir, G. Shtenberg, N. Raz, C. Gazenbeek, D. Budding, M. P. Bos and E. Segal, *Sci. Rep.*, 2016, **6**, 38099.
4 N. T. Thet and A. T. A. Jenkins, *Electrochem. Commun.*, 2015, **59**, 104–108.

5 Y. Chen, N. Cheng, Y. Xu, K. Huang, Y. Luo and W. Xu, *Biosens. Bioelectron.*, 2016, **81**, 317–323.
6 K. Rijal and R. Mutharasan, *Analyst*, 2013, **138**, 2943–2950.
7 I. Musil, V. Jensen, J. Schilling, B. Ashdown and T. Kent, *J. Med. Case Rep.*, 2010, **4**, 131.
8 Y. Xu, W. Cheung, C. L. Winder and R. Goodacre, *Anal. Bioanal. Chem.*, 2010, **397**, 2439–2449.
9 L. Váradi, J. L. Luo, D. E. Hibbs, J. D. Perry, R. J. Anderson, S. Orenga and P. W. Groundwater, *Chem. Soc. Rev.*, 2017, **46**, 4818–4832.
10 P. Mazoteras, P. J. M. Bispo, A. L. Höfling-Lima and R. P. Casaroli-Marano, *Curr. Eye Res.*, 2015, **40**, 697–706.
11 R. M. Hagen, H. Frickmann, M. Elschner, F. Melzer, H. Neubauer, Y. P. Gauthier, P. Racz and S. Poppert, *Int. J. Med. Microbiol.*, 2011, **301**, 585–590.
12 H. M. Al-Qadiri, M. A. Al-Holy, M. Lin, N. I. Alami, A. G. Cavinato and B. A. Rasco, *J. Agric. Food Chem.*, 2006, **54**, 5749–5754.
13 X. Yu, W. Jiang, Y. Shi, H. Ye and J. Lin, *J. Cell Mol. Med.*, 2019, **23**, 7143–7150.
14 N. Singhal, M. Kumar, P. K. Kanaujia and J. S. Virdi, *Front. Microbiol.*, 2015, **6**, 791.
15 E. Tait, J. D. Perry, S. P. Stanforth and J. R. Dean, *Trac. Trends Anal. Chem.*, 2014, **53**, 117–125.
16 A. W. Boots, A. Smolinska, J. J. B. N. Van Berkel, R. R. R. Fijten, E. E. Stobberingh, M. L. L. Boumans, E. J. Moonen, E. F. M. Wouters, J. W. Dallinga and F. J. Van Schooten, *J. Breath Res.*, 2014, **8**, 027106.
17 M. K. Storer, K. Hibbard-Melles, B. Davis and J. Scotter, *J. Microbiol. Methods*, 2011, **87**, 111–113.
18 R. M. S. Thorn, D. M. Reynolds and J. Greenman, *J. Microbiol. Methods*, 2011, **84**, 258–264.
19 W. Filipiak, A. Sponring, M. M. Baur, A. Filipiak, C. Ager, H. Wiesenhofer, M. Nagl, J. Troppmair and A. Amann, *BMC Microbiol.*, 2012, **12**, 113.
20 O. Lawal, H. Knobel, H. Weda, T. M. E. Nijsen, R. Goodacre, S. J. Fowler, W. M. Ahmed, A. Artigas, J. Bannard-Smith, L. D. J. Bos, M. Camprubi, L. Coelho, P. Dark, A. Davie, E. Diaz, G. Goma, T. Felton, S. J. Fowler, J. H. Leopold, P. M. P. van Oort, P. Povoa, C. Portsmouth, N. J. W. Rattray, G. Rijnders, M. J. Schultz, R. Steenwelle, P. J. Sterk, J. Valles, F. Verhoeckx, A. Vink, I. R. White, T. Winters and T. Zakharkina, *Metabolomics*, 2018, **14**, 66.
21 R. Rocchi, M. Mascini, A. Faberi, M. Sergi, D. Compagnone, V. Di Martino, S. Carradori and P. Pittia, *Food Contr.*, 2019, **106**, 106736.
22 T. Seesaard, P. Lorwongtragool and T. Kerdcharoen, *Sensors*, 2015, **15**, 1885–1902.
23 J. W. Gardner, M. Craven, C. Dow and E. L. Hines, *Meas. Sci. Technol.*, 1998, **9**, 120–127.
24 J. Carrillo and C. Durán, *Biosensors*, 2019, **9**, 23.
25 V. Sberveglieri, E. N. Carmona, E. Comini, A. Ponzoni, D. Zappa, O. Pirrotta and A. Pulvirenti, *BioMed Res. Int.*, 2014, **2014**, 1–6.
26 O. Gould, T. Wieczorek, B. De Lacy Costello, R. Persad and N. Ratcliffe, *J. Breath Res.*, 2018, **12**, 1.
27 X. Wu, S. Xiong, Y. Gong, Y. Gong, W. Wu, Z. Mao, Q. Liu, S. Hu and X. Long, *Sensor. Actuator. B Chem.*, 2019, **292**, 32–39.
28 Ü Özsandıkcıoğlu, A. Atasoy and Ş Yapıcı, *2018 IEEE International Symposium on Medical Measurements and Applications (MeMeA)*, 2018.
29 J.-E. Haugen and I. Undeland, *J. Agric. Food Chem.*, 2003, **51**, 752–759.
30 L. Hokkinen, A. Kesti, J. Lepomäki, O. Anttalainen, A. Kontunen, M. Karjalainen, J. Aittoniemi, R. Vuento, T. Lehtimäki, N. Oksala and A. Roine, *Future Microbiol.*, 2020, **15**, 233–240.
31 D. M. Guldi and S. Fukuzumi, *J. Porphyr. Phthalocyanines*, 2002, **6**, 289–295.
32 S. Kladsomboon, C. Thippakorn and T. Seesaard, *Sensors*, 2018, **18**, 3189.
33 T. Sarkar, S. Srinives, S. Sarkar, R. C. Haddon and A. Mulchandani, *J. Phys. Chem. C*, 2014, **118**, 1602–1610.
34 S. Cui, L. Yang, J. Wang and X. Wang, *Sensor. Actuator. B Chem.*, 2016, **233**, 337–346.
35 T. Seesaard, S. Seaon, C. Khunarak, P. Lorwongtragool and T. Kerdcharoen, *11th International Conference on Electrical Engineering/Electronics*, Computer, Telecommunications and Information Technology, 2014.
36 A. Kaushik, R. Kumar, S. K. Arya, M. Nair, B. D. Malhotra and S. Bhansali, *Chem. Rev.*, 2015, **115**, 4571–4606.
37 T. Eamsa-ard, T. Seesaard, T. Kitiyakara and T. Kerdcharoen, *9th Biomedical Engineering International Conference (BMEiCON)*, 2016.
38 J. Zhu, H. D. Bean, Y.-M. Kuo and J. E. Hill, *J. Clin. Microbiol.*, 2010, **48**, 4426–4431.
39 L. D. J. Bos, P. J. Sterk and M. J. Schultz, *PLoS Pathog.*, 2013, **9**(5), 1–8.
40 M. Jünger, W. Vautz, M. Kuhns, L. Hofmann, S. Ulbricht, J. I. Baumbach, M. Quintel and T. Perl, *Appl. Microbiol. Biotechnol.*, 2012, **93**, 2603–2614.
41 C. Zscheppank, H. L. Wiegand, C. Lenzen, J. Wingender and U. Telgheder, *Anal. Bioanal. Chem.*, 2014, **406**, 6617–6628.
42 K. Y. Jain and K. S. Bhandare, *Int. J. Electron. Commun. Comput. Technol.*, 2014, **3**, 45–50.
43 P. Singjai, S. Changsarn and S. Thongtem, *Mater. Sci. Eng., A*, 2007, **443**, 42–46.
44 P. Lorwongtragool, A. Wisitsoraat and T. Kerdcharoen, *J. Nanosci. Nanotechnol.*, 2011, **11**, 10454–10459.
45 T. Jayasree, M. Bobby and S. Muttan, *J. Med. Biol. Eng.*, 2015, **35**, 759–764.
46 R. Rusinek, M. Gancarz and A. Nawrocka, *LWT*, 2020, **117**, 108665.
47 A. Šetkus, A.-J. Galdikas, Ž.-A. Kancleris, A. Olekas, D. Senulienė, V. Strazdienė, R. Rimdeika and R. Bagdonas, *Sensor. Actuator. B Chem.*, 2006, **115**, 412–420.
48 Y. Zhu, Y. Zhao, J. Ma, X. Cheng, J. Xie, P. Xu, H. Liu, H. Liu, H. Zhang, M. Wu, A. A. Elzatahry, A. Alghamdi, Y. Deng and D. Zhao, *J. Am. Chem. Soc.*, 2017, **139**, 10365–10373.
49 S. Kladsomboon, M. Lutz, T. Pogfay, T. Puntheeranurak and T. Kerdcharoen, *J. Nanosci. Nanotechnol.*, 2012, **12**, 5240–5244.

50 M. E. Zhussupov, *International Journal of Fundamental Physical Sciences*, 2014, **4**, 62–71.
51 H. M. Jeon, J. Y. Lee, G. M. Jeong and S. I. Choi, *PloS One*, 2018, **13**(7), 1–9.
52 H. Fan, V. H. Bennetts, E. Schaffernicht and A. J. Lilienthal, *Sensor. Actuator. B Chem.*, 2018, **259**, 183–203.
53 E. Desimoni and B. Brunetti, *Pharm. Anal. Acta*, 2015, **6**, 355.
54 K. A. Hettinga, H. J. F. Van Valenberg, T. J. G. M. Lam and A. C. M. Van Hooijdonk, *J. Dairy Sci.*, 2008, **91**, 3834–3839.
55 H. T. Ngo, K. Minami, G. Imamura, K. Shiba and G. Yoshikawa, *Sensors*, 2018, **18**(5), 1–11.
56 A. Dey, *Mater. Sci. Eng. B*, 2018, **229**, 206–217.
57 K. Timsorn, T. Thoopboochagorn, N. Lertwattanasakul and C. Wongchoosuk, *Biosyst. Eng.*, 2016, **151**, 116–125.
58 K. Wiesner, M. Jaremek, R. Pohle, O. Von Sicard and E. Stuetz, *Procedia Eng.*, 2014, **87**, 332–335.
59 P. Pletnev, I. Osterman, P. Sergiev, A. Bogdanov and O. Dontsova, *Acta Naturae*, 2015, **7**, 22–33.
60 S. C. Becerra, D. C. Roy, C. J. Sanchez, R. J. Christy and D. M. Burmeister, *BMC Research Notes*, 2016, **9**, 216.
61 T. J. Silhavy, D. Kahne and S. Walker, *Cold Spring Harbor Perspect. Biol.*, 2010, **2**, a000414.